Prototyping electronics and software for a spectrometer module

Jimi Juola

School of Electrical Engineering

Thesis submitted for examination for the degree of Master of Science in Technology.

Helsinki 25.7.2017

Thesis supervisor:

Prof. Raimo Sepponen

Thesis advisor:

M.Sc. Erkki Seppäläinen

Aalto University
School of Electrical
Engineering

AALTO UNIVERSITY
SCHOOL OF ELECTRICAL ENGINEERING

ABSTRACT OF THE
MASTER'S THESIS

Author: Jimi Juola

Title: Prototyping electronics and software for a spectrometer module

Date: 25.7.2017 Language: English Number of pages: 8+54

Department of Electrical Engineering and Automation

Professorship: S-66 Applied Electronics

Supervisor: Prof. Raimo Sepponen

Advisor: M.Sc. Erkki Seppäläinen

A spectrometer is a device that measures properties of light at selected wavelengths. In this thesis, electronics and software are prototyped for a Hamamatsu C12880MA spectrometer module. The aim of the thesis was to design a spectrometer that is customizable according to customer's needs. This was met by designing and building a device and a software that interfaces with the spectrometer module, digitizes the measured spectrum, and transfers it to a computer. Software on the computer displays the spectrum and colorimetric values related to it. The capabilities of the device were tested by measuring various reference light sources, and the results showed that, for the most part, the device was working as expected.

Keywords: spectrometer, electronics design, microcontroller, analog to digital conversion, colorimetry

AALTO-YLIOPISTO
SÄHKÖTEKNIIKAN KORKEAKOULU

DIPLOMITYÖN
TIIVISTELMÄ

Tekijä: Jimi Juola

Työn nimi: Elektroniikan ja ohjelmiston kehittäminen spektrometrimoduulia varten

Päivämäärä: 25.7.2017 Kieli: Englanti Sivumäärä: 8+54

Sähkötekniikan ja automaation laitos

Professuuri: S-66 Sovellettu elektroniikka

Työn valvoja: Prof. Raimo Sepponen

Työn ohjaaja: DI Erkki Seppäläinen

Spektrometri on laite, joka mittaa valon ominaisuuksia tietyillä aallonpituuksilla. Tässä työssä kehitettiin elektroniikka ja ohjelmisto Hamamatsu C12880MA -spektrometrimoduulia varten. Työn tavoitteena oli suunnitella spektrometri, joka on mukautettavissa asiakkaan tarpeiden mukaisesti. Työssä suunniteltiin ja rakennettiin laite ja ohjelmisto, jotka toimivat spektrometrimoduulin kanssa, digitoivat mitatun spektrin ja siirtävät sen tietokoneelle. Tietokoneohjelma näyttää mitatun spektrin ja siihen liittyviä kolorimetrisiä arvoja. Laitteen suorituskykyä testattiin mittaamalla eri mittanormaalivalolähteitä, ja saatujen tulosten perusteella laite toimi pääosin odotetulla tavalla.

Avainsanat: spektrometri, elektroniikkasuunnittelu, mikrokontrolleri, analogia-digitaalimuunnos, kolorimetria

Preface

I would like to thank Professor Raimo Sepponen and my instructor Erkki Seppäläinen for their guidance.

I also would like to thank my colleagues for their help with the tricky problems I encountered.

Finally, I would like to thank Skunk Developments Oy for the opportunity to work with this project.

Helsinki, 25.7.2017

Jimi Juola

Contents

Abbreviations

AD	analog-to-digital
ADC	analog-to-digital converter
ARM	Advanced RISC Machine
CIE	International Commission on Illumination Commission Internationale de l´Eclairage
CMOS	complementary metal–oxide–semiconductor
CPU	central processing unit
CSV	comma-separated values
DAC	digital-to-analog converter
DMA	direct memory access
DNL	differential nonlinearity
EMC	electromagnetic compatibility
ESR	equivalent series resistance
FPGA	field-programmable gate array
FWHM	full width at half maximum
GCC	GNU Compiler Collection
GUI	graphical user interface
I^2C	Inter-Integrated Circuit
IC	integrated circuit
IDE	integrated development environment
INL	integral nonlinearity
I/O	input/output
LCD	liquid-crystal display
LED	light-emitting diode
LSB	least significant bit
LVDS	low-voltage differential signaling
MOSFET	metal–oxide–semiconductor field-effect transistor
MSPS	megasamples per second

op-amp	operation amplifier
PC	personal computer
PCB	printed circuit board
PWM	pulse-width modulation
RMS	root mean square
RSS	root sum squared
SAR	successive approximation register
SCT	state configurable timer
SMA	Subminiature version A
SPI	Serial Peripheral Interface
TUE	total unadjusted error
USB	Universal Serial Bus
UV	ultraviolet

1 Introduction

1.1 Background

A spectrometer is a device that measures properties of light at selected wavelengths. There are several low-cost spectrometers in the market, but those are typically developed for general purpose usage and not suitable for modifications. By using an off-the-shelf spectrometer module and developing a custom electronics for that, the device can be customized according to specific needs. Such needs may include size or power consumption limitations and a requirement for automatic operation.

1.2 Aims and objectives

The aim of this thesis was to develop a commercial product for Skunk Developments Oy, based on an off-the-shelf spectrometer module. The device should meet the following requirements:

- measures the spectrum of visible light on a broad range of light intensities
- is small and lightweight
- the electronics are customizable according to customers' needs
- has a minimal user interface on the device itself
- has an extensive user interface on a PC or a mobile device.

The main part of the device is a Hamamatsu C12880MA spectrometer module [26], with a measurement range of 340 nm to 850 nm. The rest of the device consists of supporting electronics such as a microcontroller and an analog-digital converter. The software has the capability to control the spectrum measurement process, and also processes and analyzes the measured spectrum data.

In order to achieve this aim, the objectives of this study were to:

- study how light is quantified
- study how a spectrometer works, focusing on the Hamamatsu C12880MA spectrometer module
- study the requirements for measurement electronics
- design and build a spectrometer device
- run a series of measurements to ensure that the device works as intended

1.3 Content of thesis

The content of this thesis consists of two main parts. The first part discusses the theory behind the device, such as how the spectrometer works, how light is quantified and what should be taken into consideration with the electronics. Even though the device won't necessarily be used for photometric measurements, that is measuring light as the human eye sees it, it is likely. For that reason, the discussion is weighted towards photometry, with the inclusion of photometric theory.

The second part describes the process of prototyping the electronics and the software for the device. As is common in electronics, multiple hardware revisions were needed. New revisions were made until the requirements were met. The process of designing electronics includes several decisions and compromises, most of which have been explained in the thesis. Finally, multiple measurements are made with the device, showing both expected and unexpected results.

2 Background

2.1 Brief history of spectrometry

Sir Isaac Newton demonstrated in 1671 that using a prism, white light can be decomposed into several different colors [45]. He is often regarded as the first one to observe the sun's spectrum, but several scientists had described that before him. Newton did, however, find out that using a slit before the prism improves the resolution of the spectrum. He also coined the term spectrum. [19, 45, 11, pp. 1–3].

In 1785 David Rittenhouse made the first diffraction grating, but it was not used for scientific experiments. Almost 40 years later, in 1821, Joseph von Fraunhofer began experimenting with diffraction gratings and using them in spectroscopy. About 1870, L.M. Rutherfurd developed gratings that were more powerful than the best prisms available. [54, p. 16]

In the early days of spectroscopy, the results could be captured in photographs, but the only method of quantifying light intensities was visual. In 1901 H. Kreusler described the first photoelectric spectrophotometer, which used a photoemissive cell as a detector. The first commercial spectrometer that was produced on a large scale was designed in 1941 by Cary and Beckman. [11, pp. 10–16]

2.2 Measuring light

As previously mentioned, the device uses a Hamamatsu C12880MA spectrometer module [26]. This 2.5 cm^3 component has an integrated slit, a diffraction grating and a CMOS linear image sensor (Figure 1).

The light entering the spectrometer reflects from the diffraction grating and is directed to the CMOS linear image sensor, which then converts the diffracted light into voltage. The image sensor has 288 light sensitive cells, pixels, which are read one by one with an ADC to the memory of a microcontroller. This yields to an average spectral resolution of 9 nm per pixel. [26] Further analysis of the spectroscopic data is done on a remote device, which is discussed on Section 3.

2.3 Market research

There are several low-cost spectrometers on the market, but those are typically developed for general purpose usage, e.g. for lighting measurements. By using an off-the-shelf spectrometer module and developing a custom electronics for that, the device can be customized according to specific needs. Such needs may

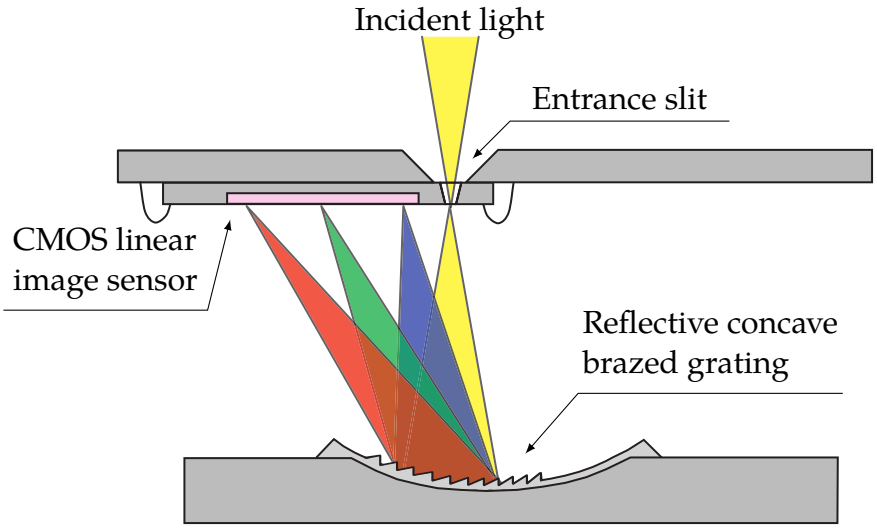

Figure 1: The optical component layout of Hamamatsu C12880MA spectrometer module. (Image reproduced with permission of Hamamatsu Photonics) [26]

include size or power consumption limitations and a requirement for automatic operation.

For about 2000 euros one can get either a handheld spectral light meter (Table 1) or a low-end laboratory spectrometer (Table 2). The typical spectral light meter has a spectral resolution of 10 nm and a color touchscreen for user interface. A cosine corrected entrance optic enables illuminance measurements. Software on the device allows the user to determine various parameters of light, such as color rendering index, correlated color temperature, and tristimulus values.

The typical laboratory spectrometer has a spectral resolution of 1 nm and needs to be connected to a computer via USB. It has an SMA connector for an optical fiber input. A software on the PC allows the user to perform various different spectral analyses.

The device designed in this thesis has a spectral resolution of 9 nm and requires a computer for operation. At its current state, it has neither properly calibrated cosine corrector nor an SMA connector, although both are possible. Cosine correctors can be bought from optical component suppliers, and Hamamatsu offers C12880MA-10, which is the same spectrometer but with an SMA connector. [26]

Table 1: Some of the competing handheld spectrometers on the market.

Manufacturer Model	Lighting Passport Standard	Konica Minolta CL-70F	Gigahertz-Optik MSC15	UPRtek CV600	GOSSEN MAVOSPEC BASE
Spectral range (nm)	380–780	380–780	360–830	380–780	380–780
Spectral resolution (nm)	8	—	10	12	—
Measuring range (lx)	5–50 000	1–200 000	1–350 000	5–70 000	10–100 000
User interface	Mobile phone	Color touchscreen	Color touchscreen	Color touchscreen	Color screen
Size (cm^3)	65	360	322	276	250
Weight (g)	77	230	160	225	200
Price (USD/EUR)	2000	2300	1500	1500	2100
Sources	[1]	[37, 67]	[22]	[69, 10]	[23, 9]

Table 2: Some of the competing low-cost laboratory spectrometers on the market and the device described in this thesis.

Manufacturer Model	Ocean Optics STS-VIS	Thorlabs CCS100	Edmund Laboratory Spectrometer	This thesis
Spectral range (nm)	350–800	350–1000	380–750	340–850
Spectral resolution (nm)	1	0.5	2.3	9
Measuring range (lx)	—	—	—	0.3–17 000
User interface	Computer (USB)	Computer (USB)	Computer (USB)	Computer (USB)
Size (cm^3)	40	293	232	114
Weight (g)	60	400	340	72
Price (USD/EUR)	1500	1800	1700	approx. 1000
Sources	[51, 60]	[66, 65]	[17]	

2.4 Use cases

The literature contains a few examples where Hamamatsu C12880MA or its predecessor C12666MA has been used.

Uto et al. [71] developed a hyperspectral imager for remote sensing via unmanned aerial vehicles. The imager is based on a scanning mechanism, where the main components are an array of spectrometers, optical fiber bundle, and a swing mirror. The device was successfully used to map the spatial distribution of agar, coralline, and sand on a seafloor.

Chew et al. [13] demonstrated a spectrally tunable light. The light consists of 38 LEDs of eight different colors, a microcontroller, and a spectrometer. By using a closed-loop feedback system, the light was able to replicate the spectrum of a cool white LED and a warm white LED.

Das et al. [15] demonstrated a wireless smartphone spectrometer for rapid, non-destructive testing of fruit ripeness. The device measures UV fluorescence from chlorophyll present in the skin of a fruit. Since the ripeness of fruits can be correlated to chlorophyll levels, the device was able to measure the ripeness of different varieties of apples.

Ramírez-Pérez et al. [56] evaluated the performance of a hyperspectral transmissometer for oceanographic applications. A transmissometer measures the optical properties of natural waters. This submersible device has a LED array and a spectrometer, and the water column between them.

3 Quantifying light and analyzing spectral data

The electromagnetic spectrum contains electromagnetic waves of all frequencies, or in other words wavelengths. Light is the part of the electromagnetic spectrum that is visible to the human eye. [40, p. 1] There is no strict range for visible light, but in literature it varies from 360–400 nm to 740–830 nm. [40, p. 2, 78, p. 1054, 25, p. 29, 42, p. 3]

3.1 Human eye

The retina of the human eye has specialized cells, photoreceptors, which are light sensitive. There are two types of photoreceptors: rods and cones. Rod cells are more light sensitive than cone cells and make seeing in dim light possible. The eye uses rods to process light when light levels range from luminances of approximately $10^{-6}\,\mathrm{cd/m^2}$ to $100\,\mathrm{cd/m^2}$. However, as rods are sensitive over the entire visible spectrum, they produce no color information, and this so called scotopic vision is monochromatic.

Brighter light stimulates cones. There are three different types of cone cells, which are sensitive to red, green, and blue colors. This allows humans to distinguish different colors when the lighting is sufficient. The luminance range for cones is approximately $0.001\,\mathrm{cd/m^2}$ to $10^6\,\mathrm{cd/m^2}$. This is called photopic vision. [68, p. 584, 40, pp. 14–15, 59, pp. 275–276]

3.2 Basic radiometric and photometric units

Radiometric units represent physical quantities of light, such as the number of photons, photon energy, and optical power. However, since the human eye isn't a perfect, linear sensor, these units won't tell how light is perceived by a human being. This is why photometric units are used as well, as they take into account how the eye senses light. [59, p. 277]

According to Wyszecki and Stiles [74, p. 259], "photometric quantities, whose measurements are most often required in practice" are luminous flux, luminous intensity, luminance, and illuminance .

The luminous flux (unit: lumen, lm) represents the total perceived power of a light source. The luminous intensity (unit: candela, cd) is a measure of the perceived power a light source in a particular direction per unit solid angle. 1 candela equals 1 lumen per steradian.

The illuminance (unit: lux, $\mathrm{lm/m^2}$) is the luminous flux incident per unit area. It measures how much incident light is striking a surface which area is known.

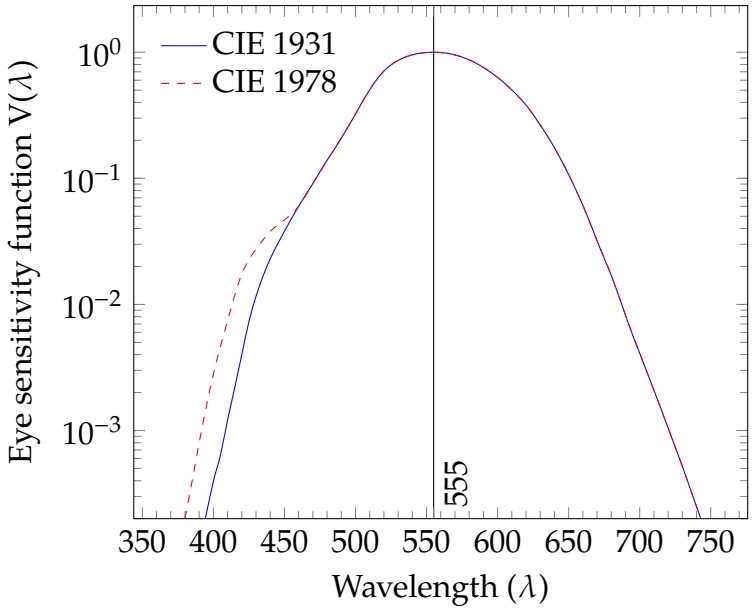

Figure 2: Comparison of the CIE 1931 and the CIE 1978 eye sensitivity functions. The maximum sensitivity of photopic vision at 555 nm is highlighted. [59, pp. 281,290]

The luminance (unit: cd/m^2) is a measure of the luminous intensity emitted in a given direction per the projected surface area in that direction. [74, pp. 787–788, 59, p. 278]

3.3 Eye sensitivity function

The luminous sensitivity of the eye isn't a constant across the wavelength of light. The eye is most sensitive to light at 555 nm for photopic vision and at 505 nm for scotopic vision. [40, pp. 14-16]

The eye sensitivity function describes the light sensitivity of the average human eye as a function of wavelength. The International Commission on Illumination (CIE) standardized the eye sensitivity function the first time in 1931. This function is referred to as the CIE 1931 $V(\lambda)$ function. [59, p. 280]

Since the function is determined by subjective measurements, it has been modified later on. More recent measurements have revealed that the CIE 1931 $V(\lambda)$ function underestimates the human eye sensitivity in the blue and violet spectral region. The modified version corrects this and is referred to as the CIE 1978 $V(\lambda)$ function. Both functions are visualized in Figure 2. [59, p. 280]

Radiometric and photometric units can be converted from one to another using the eye sensitivity function.

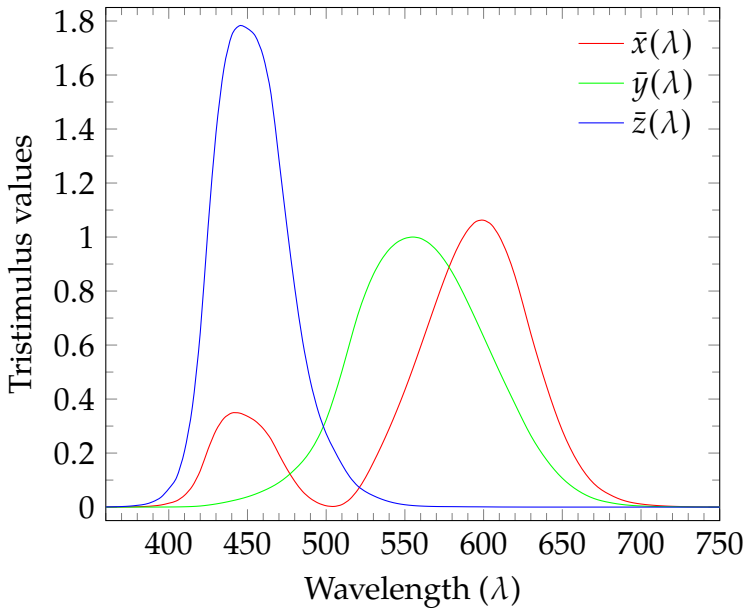

Figure 3: The CIE 1931 color matching functions. [59, pp. 293,304]

3.4 Color-matching functions and chromaticity diagram

The human eye is not able to distinguish between two lights sources of same color but different spectrum. For example, orange color can be produced by a monochromatic light source or by mixing red and yellow light sources, while the perceived color stays the same. [40, p. 3]

Any perceived color can be described by just three variables, which are calculated from the spectrum using color matching functions:

$$X = \int_\lambda \bar{x}(\lambda)P(\lambda)d\lambda \qquad Y = \int_\lambda \bar{y}(\lambda)P(\lambda)d\lambda \qquad Z = \int_\lambda \bar{z}(\lambda)P(\lambda)d\lambda \tag{1}$$

where X, Y and Z are tristimulus values, $P(\lambda)$ is the color stimulus function of the observed light, and $\bar{x}(\lambda)$, $\bar{y}(\lambda)$, $\bar{z}(\lambda)$ are the color matching functions visualized in Figure 3. [59, p. 294]

The color presented by the tristimulus values can be visualized converting the values to chromaticity coordinates with following equations:

$$x = \frac{X}{X+Y+Z} \qquad x = \frac{Y}{X+Y+Z} \qquad x = \frac{Z}{X+Y+Z} \tag{2}$$

where $x + y + z = 1$ [25, p. 127].

The color can now be shown on the chromaticity diagram (Fig. 4). The horseshoe shaped chromaticity diagram shows all the colors the human eye is able to perceive. Monochromatic colors are found on the perimeter of the chromaticity diagram.

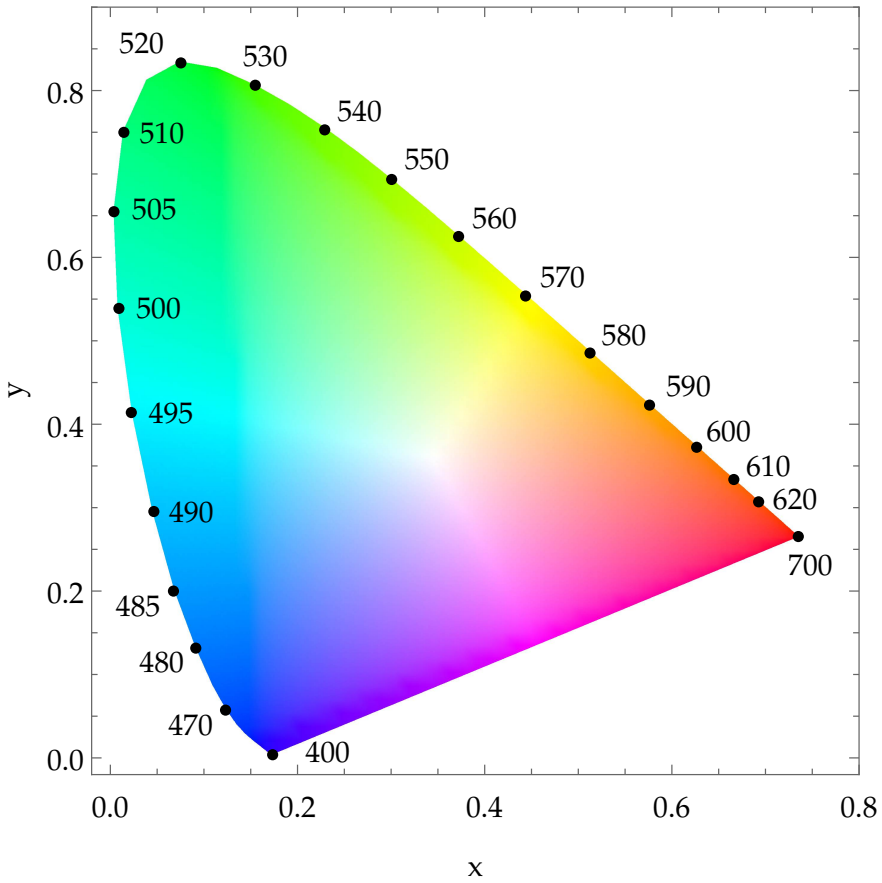

Figure 4: The CIE 1931 Chromaticity diagram. Each dot represents a single wavelength.

Colors within the diagram can be obtained by mixing two other colors. For example colors from the straight line between 400 nm and 700 nm, known as the *line of purples* can be obtained by mixing 400 nm blue and 700 nm red in a certain ratio. The colors used in mixing don't have to be monochromatic colors, the only requirement is that the color lies within the horseshoe. [59, p. 295, 40, p. 84, 57, p. 35]

3.5 Color temperature

White light can be generated from several different color combinations, and thus from several different spectrums. Planckian blackbody radiation is often used as a standard white light source, as its spectrum can be expressed using only one parameter, the color temperature. Additionally, both the sun and incandescent lights closely approximate the Planckian spectrum.

The color temperature relates to the temperature of a Planckian blackbody radiator. At lower temperatures it glows red, but as the temperature increases, the glow

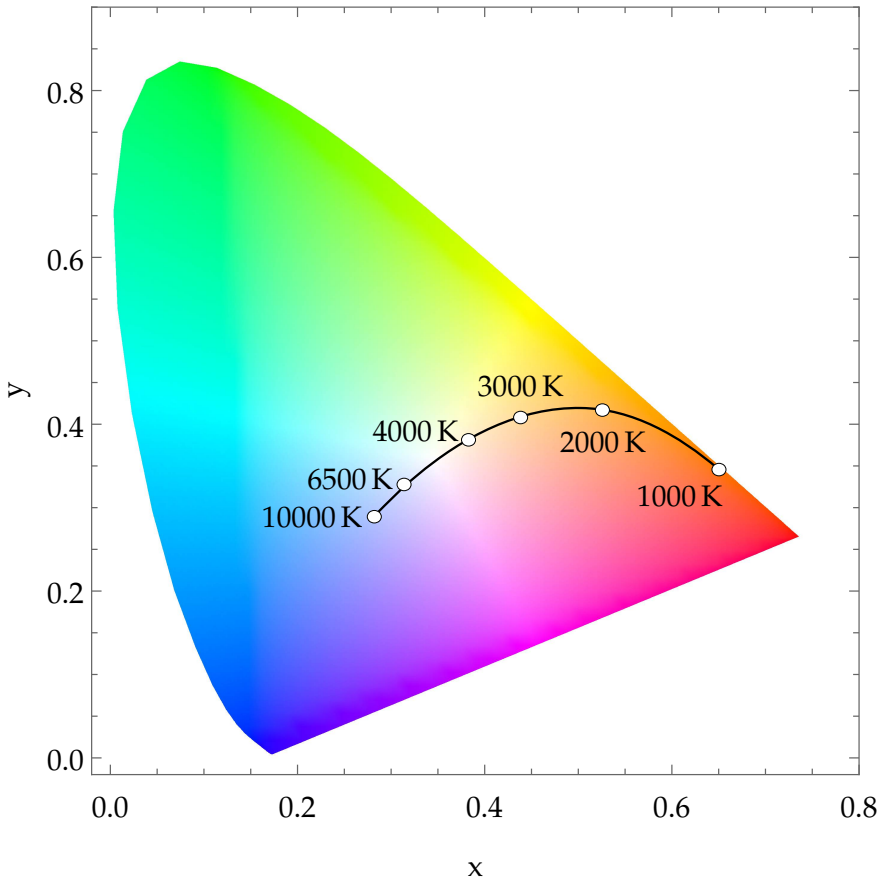

Figure 5: Chromaticity diagram containing a Planckian locus and several color temperatures.

changes to yellow, white and continuing to blue, following Wien's law. These colors and their respective temperatures can be plotted on the chromaticity diagram (Fig. 5). The arc they form is called a Planckian locus.

The color temperature of a white light source can be found out by calculating the chromaticity coordinates and determining where on the Planckian locus the coordinates fall. If they don't fall on the locus, the temperature of a Planckian blackbody radiator whose color is closest to the color of the white light source is used. This is called a correlated color temperature. [59, pp. 306–311]

3.6 Color rendering

The color temperature is not the only important parameter of white light. The spectrum of the light influences to its abilities to show the true colors of physical objects. Two lights may both look white, but have a different spectrum and thus they differ in their color rendering. This is measured in terms of the color rendering index.

In order to evaluate the color rendering ability of a light source, a reference light source is needed. The reference source should be a Planckian black-body radiator, which color temperature should match the test light source. A Planckian black-body radiator is used, as it closely resembles daylight, which understandably renders colors as people expect. As a Planckian black-body is used as a reference, it has a color rendering index of 100 out of 100.

The test light source and the reference light source are used to illuminate test color samples. The CIE has standardized a set of 14 color samples, of which eight are used in calculating the CIE 1974 general color rendering index. Those eight colors have moderate saturation and equal lightness.

The color rendering index is calculated by quantifying how much the perceived color of a color sample changes when it is illuminated first with the reference light source and then with the test light source. The procedure is repeated for each of the color samples. If there is no color change, the color rendering index for that sample is 100. The larger the change, the smaller the index will be. These sample-specific color rendering indexes are averaged, resulting in the color rendering index of the test light source.

The process can be done without any real color samples or a reference light source, as long as the spectrum of the light sources and the spectral reflectivity of the color samples are known. [74, pp. 173–175, 59, pp. 315–324, 52, pp. 465–470]

4 Electronics

4.1 ADC

An analog to digital converter is a device that converts analog signals into a digital form. Since the spectrometer module outputs the measured light level by varying the output voltage, an ADC has to be used for the acquisition of the light level information.

There are several different methods for converting analog signals to digital, each having its own advantages and disadvantages. The most common method is the successive approximation register (SAR) technique. The basic operation of an SAR ADC is simple. The sampled signal is fed from a sample-and-hold circuit to a comparator, which another input is connected to a digital to analog converter. The DAC is typically based on a charge-redistribution method, where a binary-weighted capacitor array is used to generate the required voltage. At first, the DAC output is at $V_{ref}/2$, where V_{ref} is the reference voltage. If the sampled signal is higher than V_{ref}, the most significant bit of the result is 1, otherwise it is 0. The DAC output is adjusted accordingly, a new comparison is made, and so on, until the least significant bit of the DAC is set. At this point the conversion is complete, and the value of the DAC is equal (within the limits of accuracy) to the input signal. With these successive approximations, the ADC performs a binary search over the sampled signal in order to determine its value. [34, p. 3.53]

ADCs have several different kinds of errors and non-linearities. On an SAR ADC, the overall accuracy and linearity is determined primarily by the internal DAC [34, p. 3.55]. These errors are usually expressed in terms of the least significant bit (LSB) of the data converter. Values that are specified in LSB can be converted to volts using the following formula: [44, 61, p. 27]

$$\text{volts} = \text{error in LSB} \cdot \text{maximum input in volts}/(2^{\text{ADC resolution in bits}}) \quad (3)$$

Kester et al. [35, p. 2.15] describe offset and gain errors as follows: "The transfer characteristics of both DACs and ADCs may be expressed as a straight line given by D = K + GA, where D is the digital code, A is the analog signal, and K and G are constants. [. . .] The offset error is the amount by which the actual value of K differs from its ideal value. The gain error is the amount by which G differs from its ideal value." In unipolar converters, which are the ones used in this thesis, the ideal value of K is zero. These errors can be usually trimmed algorithmically, and some converters do that automatically. There is also full-scale error, which is a sum of offset error and gain error. [35, p. 2.15, 41]

When the input of an ideal converter changes exactly 1 LSB, the digital code changes also 1 LSB. If the digital code changes before or after the exact point, the converter

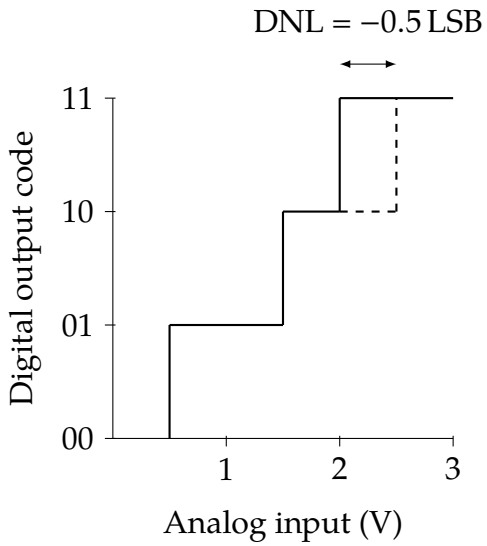

Figure 6: Differential nonlinearity error. The dotted line represents the ideal transition, the solid line represents the actual transition. The 2-bit ADC in this example has a DNL error of −0.5 LSB

has differential nonlinearity (Figure 6). [35, p. 2.17] The main reason for a DNL error is the non-idealities in the binary-weighted capacitor array, where capacitor values deviate from their ideal values [62, 24]. These deviations may be caused by imperfect design layout and variations in the die thickness [62]. A DNL error is typically defined as maximum value of DNL to be found across the entire range of the converter [35, p. 2.17].

Differential linearity is about errors in step size, while integral linearity is about the overall shape of the conversion response. The integral nonlinearity error at certain point is the sum of the differential nonlinearities from the bottom up to that particular step. [35, p. 2.108, 64, p. 7] It thus represents the linearity of the ADC.

Since DNL/INL errors are not linear and vary from device to device, there is no simple way to calibrate them. It can be done using polynomial approximations or lookup tables, for example. [4] However, in order to achieve maximum accuracy, the exact compensation has to be calculated separately for every device, due to possible variations between devices.

DNL/INL errors can be slightly reduced using averaging. This requires that the input signal has some noise in it: without noise, there would be nothing to average since the position of DNL errors doesn't change over time. This is especially effective if the DNL error is large enough that the ADC misses one code completely (known as a "missing code") at certain quantization level. With noise, some of the results are below that code and some are above, which on average results in the code that was unmeasurable. [33]

The total error of an ADC indicates how large the worst RMS error is. If no gain or offset error correction is applied, the error is called total unadjusted error (TUE). The total error is calculated by squaring the individual error terms, summing them and taking the square root of the result. This method is called root sum squared (RSS). [44, p. 5, 41]

$$E_{total} = \sqrt{{E_{offset}}^2 + {E_{gain}}^2 + {E_{inl}}^2} \tag{4}$$

The method is the best for estimating the overall error when all error sources are uncorrelated. Another method is to add all error sources together, which gives the highest possible error. The actual overall error is somewhere between the RSS and the worst-case results, often being closer to the RSS result. [41]

4.2 Voltage reference

An ADC uses a reference voltage to determine the value of the sampled voltage, by comparing the sampled voltage to the reference voltage. An ADC can have an integrated voltage reference, but semiconductor fabrication techniques used for data converters are typically unsuitable for high-quality references. This is why a separate voltage reference source is often needed. [18]

As the reference voltage is used as a yardstick, any errors in the reference voltage are visible in the result. Voltage reference error sources include, but are not limited to [28, pp. 683–684]:

- Initial accuracy
- Long-term drift
- Temperature coefficient
- Line and load regulation

The total error of a voltage reference should be sufficiently low so that the error is not significant compared to the ADC error. Edno [18] mentions that “matching the worst-case reference error to the maximum [ADC] gain error is a reasonable starting point.” The worst-case error can be calculated by summing the maximum value of each error source and then taking the log base-2 of the result. If only a typical error is specified, Edno suggests multiplying the value with three to obtain a ballpark estimate of the worst-case error. [18]

4.3 Electromagnetic compatibility

Electromagnetic compatibility (EMC) is the device's ability to function as intended in an electromagnetic environment and thus it should not be affected by any external electromagnetic sources. It should also not cause any electromagnetic interference to that electromagnetic environment, meaning it should not itself be a source of electromagnetic noise. EMC should be considered throughout the design, as the earlier possible EMC problems are found, the easier and cheaper fixing them typically is. The effect of noise on the device can be lessened by component selection, component placement, and PCB design, for example. [53, pp. 3–5]

The typical path for noise is from a noise source, via a coupling channel to a receptor. When eliminating a noise problem, the first step is to understand the noise path and the characteristics of the noise. The noise path can be broken by changing the characteristics of the noise, making the receptor insensitive to noise or eliminating the transmission through the coupling channel. [53, pp. 30–31]

As the spectrometer has both digital and analog components, a special attention should be paid to the PCB layout, so that high-speed digital currents won't disturb analog signals [53, p. 660]. Both the theory and the practice of a mixed signal PCB layout are detailed in the section 5.4.1.

5 Developing the prototype

5.1 Background and requirements for the device

One of the requirements for the device was a high dynamic range. This means an ability to use it to measure both direct sunlight and a light of a dimly lit room. There are several ways to achieve a high dynamic range, such as by varying the integration time, having an adjustable aperture or having an image sensor with a high dynamic range.

The spectrometer module selected for the device is Hamamatsu C12880MA, as it is the smallest module on the market at the time of writing. The image sensor used in the C12880MA does not have a spectacular dynamic range as is, but the integration time can be varied, thus negating the need for an adjustable aperture. Low light measurement is easier to do since all that is needed is a long integration time. For direct sunlight, the integration time has to be short enough so that the image sensor won't saturate, otherwise a neutral-density filter has to be used.

On the C12880MA a single measurement cycle consists of an integration part and an output part. During the integration part, the image sensor captures the incident light, and the shortest possible integration period is 54 clock cycles. During the output part, the spectrometer outputs the pixel data, one pixel per clock cycle. Since the shortest possible integration period is a fixed amount of clock cycles, the shortest possible integration time (10.8 µs) is achieved only when the spectrometer module is clocked at the maximum frequency of 5 MHz. [26]

The detailed process of a single measurement, shown also in Figure 7, is as follows: A stable and constant clock signal, ranging from 0.2 MHz to 5 MHz, is supplied to the spectrometer. The integration time is as long as the pin ST is high, plus 48 clock cycles. The pin ST has to be high at least 6 cycles, but there is no upper limit, which enables long integration times.

Analog pixel signal, referred as "Video" in Figure 7, starts 87 clock cycles after the ST pin has gone low. When all 288 pixels has been clocked out, a new measurement can be started by driving the pin ST high again. The spectrometer outputs a trigger signal ("TRG") for triggering an ADC, but the trigger signal is output constantly, not only while the pixel signal is clocked out. [26] This complicates the usage of the trigger signal, which is shown later.

The analog pixel signal is first fed to a buffer amplifier in order to minimize the current consumption at the video circuitry. Excess current consumption would increase the chip's temperature and generate noise to the signal. [26, 38, p. 42] After buffering, the signal is sampled with an ADC. Since the pixel signal is accompanied with a trigger signal, the correct moment for sampling is known. This way the sample rate of the analog-to-digital conversion can be the same as the

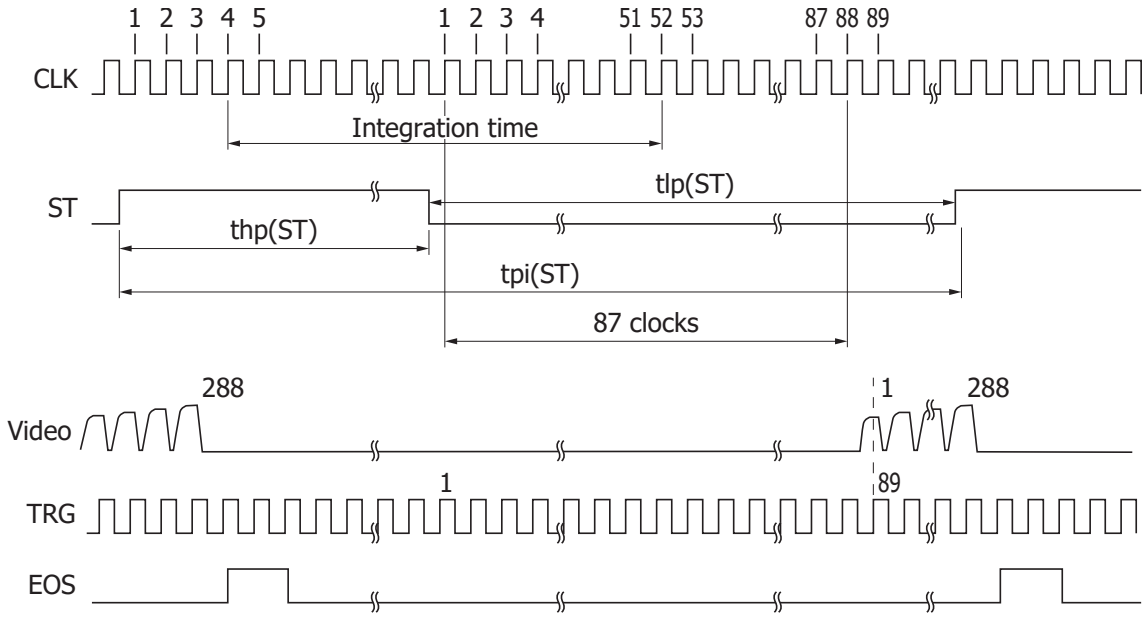

Figure 7: The timing chart of Hamamatsu C12880MA spectrometer module. (Image reproduced with permission of Hamamatsu Photonics) [26]

clock frequency of the pixel signal and no oversampling or anti-alias filtering is needed.

In order to capture the pixel data accurately, the ADC has to have a good enough resolution. The dynamic range of the C12880MA depends on the saturation output voltage and the readout noise, which are given in the datasheet: [26]

$$DR = 20\log_{10}\frac{V_{Saturation}}{V_{Noise,RMS}} = 20\log_{10}\frac{5\,\mathrm{V}}{1.8\,\mathrm{mV_{RMS}}} = 68.9\,\mathrm{dB} \tag{5}$$

The effective resolution of the ADC has to be at least:

$$\log_2\frac{V_{Saturation}}{V_{Noise,RMS}} = \log_2\frac{5\,\mathrm{V}}{1.8\,\mathrm{mV_{RMS}}} = 11.4\,\mathrm{bit} \tag{6}$$

This means the ADC has to have a nominal resolution of 14–16 bits, or otherwise it has lower dynamic range than the spectrometer. That, however, introduces an another problem: with 5 MSPS and 16 bits per sample, the data rate is 80 Mbit/s. A data rate that high is too much for most, if not all 8-bit microcontrollers or even low-end ARM processors. There are two ways to reduce the data rate, either lowering the resolution or the sample rate. Lowering the resolution can be compensated by averaging the results. Halving the resolution to 8 bits means that in order to generate a 16-bit result, one has to average 256 8-bit results. [5, p. 5] This still yields a data rate of 40 Mbit/s.

Lowering the sample rate is an easy way to reduce the data rate, but it limits the shortest achievable integration time. One of the design parameters was an ability

to measure the spectrum of the sun. Hamamatsu reports that C12880MA has a dynamic range from 600 nW/m^2 to 20 W/m^2 when measured at the wavelength of 600 nm [26, p. 4]. At 600 nm spectrometer's spectral resolution is about 9 nanometers, i.e. single pixel captures several different wavelengths. Solar spectral irradiance at the Earth's surface at 600 nm is 1.135 W/(m^2 nm) [74, p. 5], so the spectrometer should be able to capture twice as much light:

$$\frac{20\,\frac{\mathrm{W}}{\mathrm{m}^2}}{1.135\,\frac{\mathrm{W}}{\mathrm{m}^2\,\mathrm{nm}}} \cdot 9\,\mathrm{nm} = 2 \tag{7}$$

The peak solar spectral irradiance at the Earth's surface is 1.165 W/(m^2 nm) at 500 nm, which is 2.6 % higher, and the spectrometer's relative sensitivity at that wavelength is 25 % higher. It is safe to say that with the shortest integration time the Hamamatsu C12880MA spectrometer should be able to measure the sun's full visible spectrum [26, p. 3, 74, p. 5].

But how much longer the integration time can be? We can calculate that by accounting the difference in spectral irradiance and spectrometer's relative sensitivity at 500 nm:

$$\frac{20\,\frac{\mathrm{W}}{\mathrm{m}^2}/1.25}{1.135\,\frac{\mathrm{W}}{\mathrm{m}^2\,\mathrm{nm}} \cdot 1.026} \cdot 9\,\mathrm{nm} = 1.5 \tag{8}$$

The integration time, and thus the data rate can be 1.5 times lower than the maximum to be still able to measure the sun's spectrum. This results in a sample rate of 3.3 MSPS and with 16-bit samples a data rate of 53.3 Mbit/s, which is still quite high.

5.2 First prototype

The purpose of the first prototype was to evaluate the selected components and see if they performed as expected. The prototype was built on a breadboard and used a microcontroller evaluation board for simplicity and quick prototyping. The hardware block diagram is depicted in Figure 8. Software-wise at this point the only required function is transmitting the measurement to the computer.

5.2.1 Hardware

The main problem at this stage is selecting optimal components. The result is a compromise between performance, component costs, and development costs. Hamamatsu's C13016 evaluation board for the C12880MA spectrometer has been

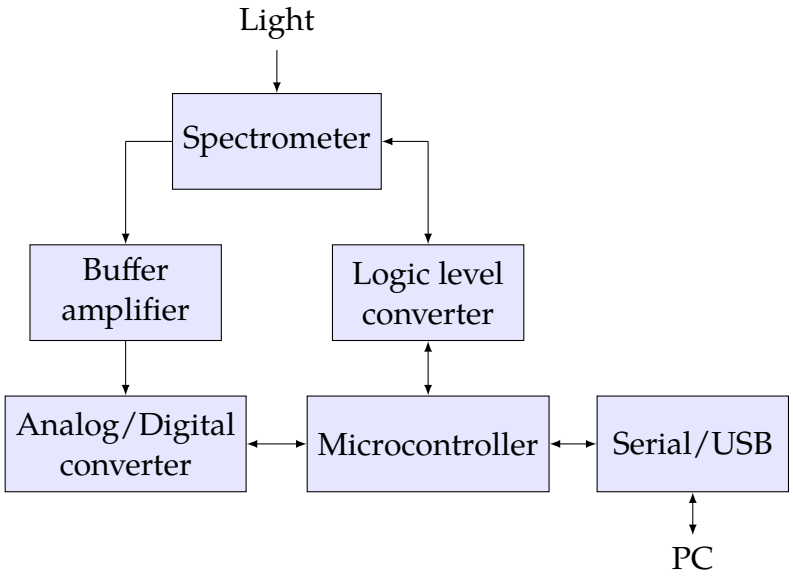

Figure 8: The hardware block diagram of the first prototype.

designed to ensure that the performance of the spectrometer is not limited by the electronics.

Although the selection process of an ADC and a microcontroller is described here separately, it was quite intertwined, as certain parameters of the selected ADC limited the choice of microcontrollers and vice versa.

Analog-to-digital converter The ADC can be either a stand-alone (a separate IC) or integrated into the microcontroller. The benefit of integration is simpler interfacing, but the performance is often lackluster compared to stand-alone ADCs. An integrated ADC can be interfaced just by writing and reading the correct registers of the microcontroller. Stand-alone ADCs have typically either a serial or parallel interface, and if the interface is serial, it is usually either an SPI or I^2C bus. Using a standardized bus simplifies interfacing, as microcontrollers often have a hardware support for them. [28, pp. 880, 1061] Another benefit of using a stand-alone ADC is that this way the ADC and the microcontroller can be chosen separately.

It was established in the Section 5.1 that the effective resolution of the ADC should be at least 11.4 bits and the sample rate should be at least 3.3 MSPS. The C13016 evaluation board uses an Analog Devices AD7961, which is a 16-bit and 5 MSPS stand-alone ADC [27]. However, this ADC costs 35 € in relatively small quantities and its high data rate requires a powerful microcontroller, and as a matter of fact, on the C13016 data processing is done by an FPGA [27]. The problem with FPGAs is that they are regarded as much more difficult to program and debug than microcontrollers [28, p. 1093]. The AD7961 uses a serial LVDS (low-voltage

differential signaling) interface, which is a high-speed interface and practically nonexistent on microcontrollers.

In the search for an optimal ADC, portfolios of Analog Devices, Linear Technology, Maxim Integrated, and Texas Instruments were sifted through. Criteria for selecting the ADC were:

- About 3.3 MSPS sampling rate
- 14–16 bits of resolution
- SPI or I^2C bus
- Price in small quantities about 10 €

One of the limiting factors is how fast the microcontroller can read and store the digitized signal from ADC's registers, as discussed later. With these criteria and limitations in mind, the selected component was Analog Devices AD7944, a 14-bit, 2.5 MSPS ADC with an SPI interface. The required SPI speed for the AD7944 operating at full speed was calculated as follows:

$$14\,\text{bit} \cdot 2.5\,\text{MSPS} = 35\,\text{Mbit/s} \tag{9}$$

which equals 35 MHz, since on an SPI bus data is transferred one bit per clock cycle. It is not fast enough to measure direct sunlight without a neutral-density filter, but faster ADCs were out of reach as they required more advanced microcontrollers. [2]

The calculated error for the AD7944 is $\pm 0.6\,\text{mV}_{\text{RMS}}$, using Equation 4 (page 15) and values from Table 4 (page 27). Since this is lower than the noise of the spectrometer ($1.8\,\text{mV}_{\text{RMS}}$), the accuracy of the ADC shouldn't be limiting the performance of the spectrometer.

Microcontroller In this application, the main criteria for selecting the microcontroller were the SPI speed and ease of development. Serial Peripheral Interface (SPI) is an IC-to-IC communication interface [28, p. 1033]. Most of the considered ADCs used an SPI bus, so high SPI speed is essential since it dictates how high sampling rate and resolution can be used. And since the device will probably be produced in relatively small quantities, the development costs should be kept as low as possible.

Developing for 8-bit microcontrollers is typically easier than for 32-bit microcontrollers, since the latter are more complex and require more setup considerations [20]. However, as Table 3 shows, 8-bit microcontrollers usually have low SPI speed. Using a 32-bit microcontroller doesn't automatically ensure high SPI speed, but some chips can have as high SPI clock as is the CPU clock.

Table 3: Microcontrollers considered for the first prototype. Max SPI speed is the maximum speed for the SPI communication. The real bit rate is usually lower, depending on the microcontroller. Abbreviations: CM0 = ARM Cortex-M0, CM0+ = ARM Cortex-M0+

Model	Family	Instruction word length (bits)	Max SPI speed (MHz)	Source
Atmel ATmega328p	AVR	8	10	[6, pp. 196, 303]
Microchip PIC18F2XK20	PIC	8	16	[43, p. 185]
Atmel SAMD09	CM0+	32	12	[8, p. 462]
NXP LPC81x	CM0+	32	30	[49, pp. 232, 245]
NXP LPC111x	CM0	32	50	[47, pp. 34, 224]

It was decided that the microcontroller should be a 32-bit one, and since all the considered 32-bit microcontrollers had an ARM core, the search was limited to ARM-based microcontrollers. ARM Holdings licenses its intellectual property cores to IC manufacturers, and they then integrate memory or a memory controller and other peripherals to the processor. This allows a large variation of peripherals between different ARM microcontrollers. [39, p. 6]

ARM has several processor families, of which Cortex-M is most suitable for this application since it is designed for low-powered microcontrollers [39, pp. 9, 11]. Further, Cortex-M has currently six versions, M0, M0+, M1, M3, M4 and M7, from least to most powerful. Cortex-M0/M0+/M1 have only 56 instructions, which allows a simpler processor design and lower power consumption. Cortex-M3 introduces a larger instruction set and additional features such as a hardware divider. These aren't necessary, as the highest computing requirement for the processor is to read data from the SPI bus to the memory as fast as possible. Cortex-M1 is optimized for FPGAs, and thus not relevant in this application. Cortex-M0+ has a couple of additional features compared to Cortex-M0, but its power consumption should be similar or slightly lower. [76, pp. 13-17, 75]

Now that the processor architecture is known, the maximum SPI bit rate can be estimated. According to Yiu [76, p. 57] "on ARM-based microcontrollers, peripherals are controlled by memory-mapped registers." This means that the SPI devices connected to the microcontroller can be accessed by a simple memory read command. The process of reading the ADC data over the SPI bus to the memory of the microcontroller was estimated to be as follows:

Read the ADC data from the memory to the processor register	2 cycles
Write the register to another memory address and increment the address	2 cycles
Check that all 288 pixels have been read	1 cycle
If not, repeat the above	2 cycles

The above cycle counts are for ARM Cortex-M0+ [3, p. 26]. Atmel AVR has the same cycle counts, except reading from an I/O to the register (the first step) is only 1 cycle [7]. There might be some unforeseen aspects that require extra cycles, but the sum of the above, 7 cycles, was thought to be the absolute minimum for a single SPI transfer. 7 cycles equals about 2.3, 4.3 and 7.1 MSPS for 16, 30 and 50 MHz clock speeds, respectively. Atmel ATmega328p, and probably all the other 8-bit AVRs as well, have an 8-bit SPI read data buffer, which lowers the bit rate [6, p. 160]. The actual bit rate depends on how the transfer of a 14 or 16-bit ADC output using an 8-bit buffer is implemented, but typically it halves the bit rate.

The main criteria for selecting the microcontroller were:

- SPI speed
- Ease of development
- Package configuration

The search was limited to Cortex-M0 and M0+ microcontrollers, since they are regarded as beginner friendly [76, p. 11]. Microcontrollers from STMicroelectronics, NXP Semiconductors, and Atmel were evaluated. From these three manufacturers, microcontrollers made by NXP had the highest SPI speeds. All three had microcontrollers with some kind of an advanced counter, capable of toggling an output pin when the counter matches a predefined value. This feature is crucial for controlling the C12880MA spectrometer, since it has relatively strict and complex timing requirements. All three also supply extensive tools for software development, including an IDE and software libraries.

With the exception of SPI speed, all of the evaluated Cortex-M0 and M0+ microcontrollers fulfilled the requirements. From the NXP microcontrollers with high SPI speed an LPC824 was chosen. It falls slightly short on SPI speed with 30 MHz compared to required 35 MHz. A faster alternative would have been LPC111x-series. However, LPC8xx-series has a benefit: it has a Cortex-M0+ core instead of Cortex-M0, and the M0+ has a single-cycle I/O for a high-speed access to peripherals [76, p. 99]. This was thought to be beneficial for timing the spectrometer and the ADC.

LPCXpresso824-MAX development board was used for developing the first prototype, as it has an ability to program and debug the LPC824 microcontroller over an USB connection.

Buffer amplifier Hamamatsu C12880MA datasheet [26, p. 2] states that "an increase in the current consumption at the video output terminal also increases the chip temperature and so causes dark current to rise. To avoid this, connect a buffer amplifier to the video output terminal so that the current flow is minimized."

Hamamatsu C13016 evaluation board for the C12880MA uses an Analog Device operation amplifier AD8092 in a voltage follower configuration [27]. AD8092 is a dual op-amp, but only one op-amp is used in buffering. The single version is AD8091. As AD8091/AD8092 is known to be suitable for the application, readily available and low-priced, was is the selected part for the device.

Logic level converter The C12880MA spectrometer requires a 5 V I/O voltage and the AD7944 ADC requires a 2.5 V I/O voltage. The LPC824 microcontroller has a 5 V tolerant I/O, meaning it can receive signals up to 5 V, but transmitted signals are at the same level as the operating voltage of the microcontroller. The operating voltage of the LPC824 was lowered from 3.3 V to 2.5 V, which made it possible to interface with the AD7944 without a level converter. For the spectrometer a simple MOSFET-based bidirectional logic level converter was used.

5.2.2 Software

The software was based on the libraries and examples provided by NXP in LPCOpen package. The development was started from controlling the spectrometer. The LPC824, as several other microcontrollers from NXP, has a state configurable timer (SCT). NXP describes it as "a powerful, flexible timer module capable of creating complex PWM waveforms and performing other advanced timing and control operations with minimal or no CPU intervention." [50, p. 257] The SCT has capabilities to toggle pins and raise interrupts when a counter matches a predefined value.

In this application, the SCT was used as two separate but synchronous 16-bit counters. The first counter was used as a clock source, and it was programmed to constantly toggle a single pin, thus generating a clock signal. This clock signal was fed to the spectrometer. The other counter was used to generate the start pulse ("ST" in Figure 7).

At this point, the output of the spectrometer could be measured with an oscilloscope. The next step was to read the video signal with the AD7944 ADC. The ADC was connected to the microcontroller and a simple conversion-acquisition loop was developed, where the ADC first converts the signal and the digital data is then transferred over the SPI bus.

Soon after, it was realized that the conversion speed of 2.1 MSPS was unachievable. 2.1 MSPS was supposedly the highest speed that was possible, but this assumption was wrong. First of all, the previously calculated CPU cycle count for transferring and storing a single ADC result was not achieved. The program was written in C and then compiled using GCC, but even the optimization level 3 of GCC was unable to produce a machine code that could do the previously mentioned

operation in just 7 cycles. Hand optimizing the code could have helped, but this was never done, as another problem was noticed.

The conversion speed of 2.1 MSPS was calculated as follows:

$$\text{SPI clock speed / ADC bit depth} = \text{samples per second} \tag{10}$$

This assumes that the ADC is capable of converting and transferring simultaneously, but it was realized that the AD7944 could not do that. The AD7944 has a so-called turbo mode, which allows some of the data transfer happen during the conversion phase, but even with that the phases when no data transfer is allowed take too long time. Using the turbo mode also complicates the SPI transfer, since a single 14-bit transfer has to be made in two parts of unequal length. The highest speed that was achieved without the turbo mode was around 1 MSPS, the turbo mode was not tried due to its complexity.

5.2.3 Conclusions from the first prototype

The problem with the first prototype was concentrating too much on material costs and too little on development costs. It would have been better to select an excessively powerful microcontroller, which would have given some extra leeway for dealing with unforeseen problems. It was thought that a more powerful microcontroller would be more difficult to program and debug, but it was later realized that this was only partially true.

5.3 Second prototype

The second prototype was built to solve the shortcomings of the first prototype. Known limiting factors were the microcontroller and the ADC, so those were replaced in the second prototype.

5.3.1 Hardware

Microcontroller The time spent on working with the LPC824 meant that microcontrollers with same or similar development tools, libraries, and internal peripherals have an advantage over other microcontrollers, since the initial learning phase would be shorter. For that reason, the search for a replacement for the LPC824 was limited to NXP's Cortex-M3s and M4s, as those had main clock speeds around and over 100 MHz. From that group the LPC54000 series was found out to be most suitable, for the following reasons:

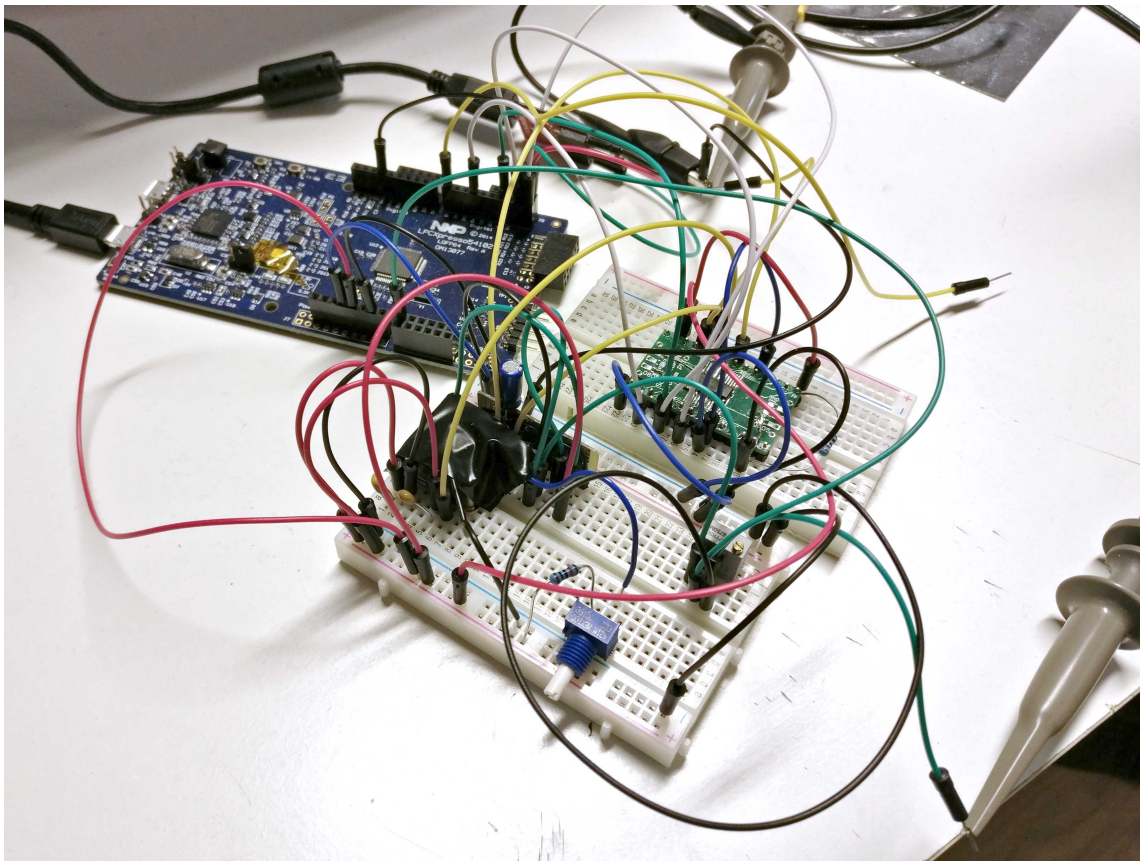

Figure 9: The second prototype.

- Integrated 12-bit ADC with conversion rate of 5 MSPS
- No unnecessary peripherals, such as Ethernet, LCD control or motor control
- Development board available
- Chip available in a leaded package

The main reason for the LPC54000 series was the fast ADC. Although the resolution of the ADC was not optimal, the conversion speed was. As mentioned earlier, the faster the conversion speed, the shorter the shortest possible exposure time. The resolution could be enhanced by averaging, but if the exposure time is too long, the image sensor will saturate and information is lost.

An additional benefit of an integrated ADC was an ability to use a direct memory access (DMA). When data is transferred using a DMA, conversion results can be stored in the memory without CPU intervention. This simplifies and speeds up continuous conversion.

The calculated error of the ADC is $\pm 6.3\,\mathrm{mV_{RMS}}$, using Equation 4 (page 15) and values in Table 4. As the noise of the spectrometer is $1.8\,\mathrm{mV_{RMS}}$, the accuracy

of the ADC is the limiting factor. The lower accuracy was a trade off for a faster conversion speed.

The selected microcontroller was NXP LPC54102 since a development board LPCXpresso54102 was available for it.

Table 4: The specified typical values for the error sources of ADCs used in this thesis. [2, 48, p. 69]

	AD7944	LPC5410x
differential nonlinearity error	±0.25 LSB	±2 LSB
integral nonlinearity error	±0.25 LSB	±2 LSB
gain error	±2 LSB	±3 LSB
offset error	±0.08 mV	±5.6 mV

Other components The buffer amplifier was the same as in the first prototype. The logic level shifter between the 3.3 V microcontroller and the 5 V spectrometer was the same as in the first prototype, a simple circuit of a single n-channel MOSFET and two 10 kΩ pull-up resistors per channel. This circuit suffered from a slow rise time, which limited its speed. Even after replacing the pull-up resistors with 1 kΩ resistors its maximum speed was about 200 kHz. Subsequently, the circuit was replaced with a Texas Instruments TXB0104, which is designed as a level shifter IC.

5.3.2 Software on the microcontroller

From the beginning, it was known that the three main parts of the software were converting the data (ADC), transferring the data (DMA) and timing the spectrometer (SCT). Fortunately, there was an open source example for the LPC824 demonstrating almost the same procedure [16]. Since the LPC54102 also uses LPCOpen, the code from the LPC824 example was relatively simple to port to the LPC54102.

The main operation of the software is following:

1. Receive the measurement parameters such as exposure time over a serial port
2. Interface with the spectrometer and read the pixel data
3. If required, repeat the above and average the results
4. If required, adjust the exposure time
5. Output the data over a serial port

Timing Timing the spectrometer was implemented in the same way as in the first prototype, using the state configurable timer (SCT) as two 16-bit counters. The first counter generated the clock signal and the second counter generated the start pulse. The second counter had three match values, for starting and ending the start pulse and for enabling the ADC. This posed a problem, as a 16-bit counter clocked at 5 MHz will wrap around after only 13.11 ms, making longer exposure times impossible.

In order to avoid this an additional timer was included. As the second counter had hit the "start the start pulse" mark, the counter was paused and a 32-bit timer was started. The timer was configured so that it will trigger an interrupt when the wanted exposure time has passed. In the interrupt handler the second counter was started again, the start pulse was ended and the ADC was enabled. Now the exposure time could be over 14 minutes long.

Trial and error with jitter In the initial tests, this method of controlling the exposure time appeared to be functioning correctly. However, after the level shifter was replaced with a faster one, as previously mentioned, and the clock frequency of the spectrometer was in the megahertz range, it was noted that the measured spectral data had intermittent jitter. The jitter did not occur every time the device was used, but when it did, every 2–10 measurement was erroneous, as the spectral data was shifted by a single pixel.

At first it was thought that the problem was caused by the interrupt that enables the ADC. The spectrometer outputs a trigger signal to indicate when the analog pixel signal should be sampled. But as shown in Figure 7, the trigger signal is output constantly, not only while the pixel signal is output. For this reason the trigger signal has to be either suppressed or ignored until the pixel signal is output. This was done by counting the clock pulses and at the right moment rising an interrupt that enabled the ADC.

ARM Cortex-M processors have, as processors commonly do, interrupt latency. When the interrupt has been requested, the processor has to stop executing the main thread and start executing the interrupt handler. There is a delay between the request and the interrupt handler execution. The exact duration of this delay depends on what the processor is executing when the interrupt is requested. This causes jitter in the interrupt response time. [77]

The reasoning behind suspecting the jitter in the interrupt response time was that there was no jitter in the measurement results when the clock frequency was low enough. This led to believe that at higher clock speeds there was such a low tolerance for interrupt latency jitter, that a different method for handling the ADC trigger signal should be developed.

The SCT can be used for manipulating pins on the microcontroller and the manipulation happens without latency at the moment when the counter matches a predefined value. The first idea was to enable and disable the spectrometer-generated trigger signal with an external switch. A two-MOSFET circuit was used, where the microcontroller switches an n-channel MOSFET, which in turn switches a p-channel MOSFET. The p-channel MOSFET was between the spectrometer and the lever shifter IC. The circuit never worked correctly, for reasons that remain unclear. The p-channel MOSFET was not able to fully close, but remained partially open, which allowed the trigger signal to start the conversion. Several different MOSFETs and circuit variations were tried, but the circuit did not function as expected.

The next choice was to use a level shifter as a switch. The TXB-series level shifters have an output-enable input, which can be used to disable all outputs of the level shifter. A single-channel version, TXB0101, was used for the tests. The tests showed that when the output is enabled, output level rises too slowly and several cycles are output before the signal level is stabilized. The level shifter datasheet confirmed this, stating that the enable time is 1 µs, equaling 5 cycles at 5 MHz. This is unacceptable since it would result in several cycles being in the forbidden zone between high and low.

At this point, it was noticed that the real reason for the jitter was not the interrupt latency, but the SCT. The SCT was split into two 16-bit counters, where the first counter generated the clock signal. The clock output pin was toggled every time the first counter changed its value, resulting the clock pulse going low when the counter had an even value and vice versa. When the start pulse went high the timer responsible for the exposure time was started. When that timer triggered an interrupt, the start pulse was lowered 48 cycles later.

The start pulse should have been lowered when the first counter had an even value, i.e. when the clock pulse was low, but there was no mechanism to ensure this and it depended only on the length of the timer. If the start pulse was lowered on an odd value, the results were shifted by one pixel. If the start pulse was lowered while the counter was about to change its value, the result was either way. With higher clock speeds the probability of lowering the start pulse while the counter was changing was higher. These are the reasons why the problem was noticed only on high clock speeds, and even then only seldom.

When the software was tested, a white LED was used as a light source, and it had a prominent blue peak in the spectrum. If the exact position of this blue peak would have been monitored, the problem with shifting would have been noticed right away.

Timing solution using the CPU clock as a clock source As the method of using two separate counters was found out to be faulty, the clock signal had to be generated by other means. The SCT is essential for timing the spectrometer, and luckily it was possible to feed an external clock source to it. An electronic oscillator was considered, but a colleague noted that ARM microprocessors usually have a possibility to output the CPU clock signal. This was found out to be the case with the LPC54102 as well, and the clock output had also a programmable divider so the correct frequency was obtainable.

The final, working configuration was to use a divided main clock as a clock source, feed that clock signal to both the spectrometer and the SCT, and to use the SCT as a single 32-bit counter. The SCT generates the start signal for the spectrometer and uses an interrupt to enable the ADC.

Automatic exposure control and averaging The automatic exposure control evaluates the measured pixel values after a complete measurement is done. If a single pixel is over a predetermined value, the complete measurement is considered as overexposed. If all pixels are under an another predetermined value, the measurement is considered as underexposed. For example, as the ADC gives values from 0 to 4095, the lower value for the exposure control could be 3000 and the upper value 4000.

If the measurement is overexposed, the exposure time is adjusted by 0.75. Respectively after an underexposed measurement the exposure time is adjusted by 1.1. When the spectrometer is demonstrated the typical change in the light intensity is a short drop. For that reason the adjustment for underexposure isn't as fast as for overexposure.

Averaging is done by a simple arithmetic mean. If both automatic exposure control and averaging are used, the averaging cycle is terminated and the exposure time is adjusted if a single overexposed pixel is encountered.

5.3.3 Software on PC

The software on the PC was written using Python and matplotlib 2D plotting library [29]. The software had two threads, one for reading the pixel data from the serial port, and the other one for updating the plot. It had an extremely simple GUI, consisting of just a plot in a window. At this point the only function was plotting the measurement.

Figure 10: The third and final prototype.

5.4 Third prototype

As the second prototype functioned as supposed, the purpose of the third prototype was to copy the electronics from the breadboard and the microcontroller development board into a single PCB.

5.4.1 Hardware

Power supply The device was designed to operate from a 5 V USB supply. The power supply should have sufficiently low noise so as not to cause noise in the spectral measurements. There are four components requiring a clean power supply: the spectrometer, the buffer amplifier, the voltage reference and the analog parts of the microcontroller. The spectrometer requires a 5 V supply voltage, so in theory it can be powered from the USB. However, USB 2.0 specifications allow the supply voltage to range from 4.75 V to 5.25 V, and the supply voltage may go as low as 4.4 V if a bus-powered hub is used [36, 70, p. 175]. Another problem was that the buffer amplifier AD8092 does not have a rail-to-rail input, meaning that in order to buffer the 5 V output signal from the spectrometer, the supply voltage for the buffer amplifier has to be at least 6 V.

The solution was to convert the supply voltage to a higher voltage, and to use a linear regulator after the switching converter to drop the voltage [28, p. 650, 32, p. 9.77]. For a switching converter a charge-pump was used. Charge-pumps are less noisy and cause less electromagnetic interference, since they use a capacitor as an energy storage instead of an inductor [28, p. 638, 32, p. 9.74].

The charge-pump used in this device was a Texas Instruments LM2665, used as a voltage doubler. The LM2665 requires only three 10 µF low-ESR capacitors and a Schottky diode. Polymer aluminum electrolytic capacitors were used due to their low ESR and high volumetric capacitance. Since the charge-pump has large switching currents, capacitors were connected to the charge-pump IC with short traces, and the components were positioned far from the analog part of the PCB.

The approximately 10 V produced by the charge-pump was lowered to 5 V using a Texas Instruments LM2937 regulator. The LM2937 was chosen since it has a 53 dB or higher power supply ripple rejection from 10 Hz to 1 MHz.

The rest of the electronics are powered by a Microchip MCP1700 voltage regulator, which generates 3.3 V from the 5 V USB supply. As the only requirements for this part were size, supply current, and output voltage, there were plenty of choices to choose from.

Buffer amplifier In the first two prototypes an Analog Devices AD8091 was used as a buffer amplifier. The signal chain was as follows:

$$\text{spectrometer module} \rightarrow \text{buffer amplifier} \rightarrow \text{voltage divider} \rightarrow \text{ADC}$$

This ensures that the spectrometer output is not excessively loaded. The voltage divider drops the signal amplitude from 5 V to 3.3 V. A 500 Ω trimmer potentiometer was used as a voltage divider, but it had too high impedance for the ADC. High source impedance resulted in excessive noise, as the sampling capacitor of the ADC did not fully charge during the sample-and-hold cycle. This was confirmed by rising the sampling time and lowering the sample rate, which resulted in a lower noise level.

In the third prototype this problem was sorted out by using a second buffer amplifier, which was between the voltage divider and the ADC. An Analog Devices AD8092 was used for this, which is essentially a dual-package AD8091, so only single IC was needed.

Voltage reference The previous prototypes have not used a separate voltage reference. Instead the supply voltage has been used as a reference. The problem with this method is that the supply voltage is typically noisy, and hence unsuitable for measurements requiring high accuracy.

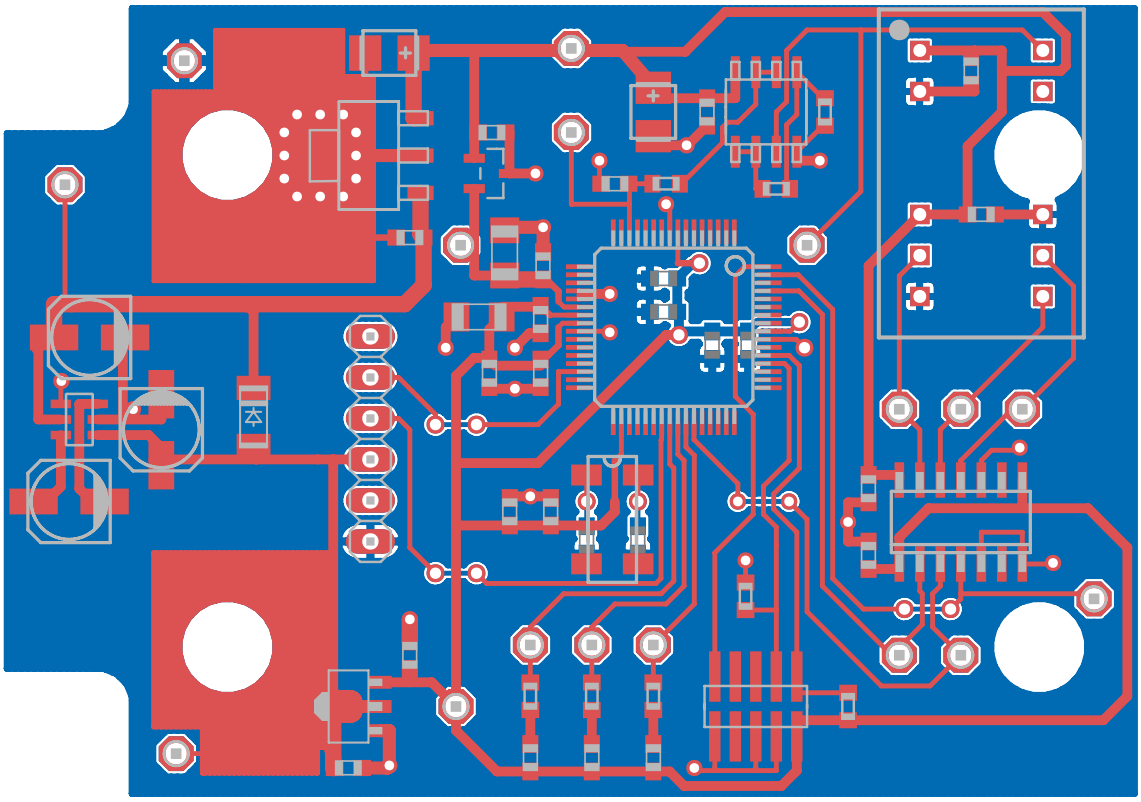

Figure 11: The PCB layout of the third prototype. The PCB has been laid out so that high speed digital signals disturb analog signals as little as possible. The spectrometer module is in the top-right corner, and the whole quadrant is reserved for analog signals. In the middle is the microcontroller and on the left side are power supply components, a charge pump and two regulators.

The voltage reference chosen for the third prototype was a Texas Instruments REF3033. Using methods described in [18], the worst-case accuracy loss due to reference error was calculated as 3 LSB, assuming that the operating temperature range is from 20 °C to 35 °C and the spectrometer is calibrated. The magnitude of the error is the same as the gain error of the ADC, as recommended in situations where there is no knowledge how large the reference error should be [18].

Microcontroller's reference voltage supply has 0.1 µF and 10 µF ceramic capacitors for bypassing, as recommended by the LPC54102 datasheet [48, p. 76].

PCB and layout The printed circuit board is a mixed-signal board since it has both analog and digital signals. In an optimal situation the board would have six layers, in the following order:

1. Analog signals
2. Analog power plane

3. Analog ground plane
4. Digital signals
5. Digital ground plane
6. Digital power plane

This way signal layers are adjacent to a plane, power and ground are adjacent to each other and high-speed digital signals are between ground planes, so that the ground planes act as shields and reduce radiated emissions. Also, analog and digital signals are completely separated to their own layers, and thus high-speed digital signals won't disturb analog signals. [53, pp. 637-648,681-682]

In order to reduce both development and manufacturing costs, the PCB has only two layers. With two layers there can be only one ground plane, so special consideration was necessary to keep the digital noise away from the analog signals. One way of separating the signals is to isolate the analog and the digital grounds by physically splitting the ground plane in two. These two sections have to be connected at some point to ensure that they share a common ground. The point of connection is typically under the ADC. The problem with a split ground plane is that no trace can be routed over the split, but only over the connected point, which would've been practically impossible. If a trace is routed over the split, the return current would have to travel all the way through the connected point, creating a large ground loop area. [53, pp. 660-686]

Instead, analog and digital signals were separated by partitioning, i.e. keeping the respective signal traces in their own partitions. There is a single ground plane covering the whole PCB, which allows much more flexible trace routing. The upper part of the PCB, shown in Figure 11, is the analog section, containing the spectrometer, the buffer amplifier, and the voltage reference. This part of the board has no traces that carry high-speed digital currents. [53, pp. 660-686]

The ground plane has been kept as solid as possible, as slots in the ground plane cause return path discontinuities. As with the split ground plane, if a trace is routed over a slot, the return current must flow around the slot. This, in turn, increases the PCB radiation and may lead to EMC problems. [53, pp. 627-628] The PCB has a couple of places where routing over a slot was unavoidable, but in those cases, the width of the slot has been kept at a minimum.

Enclosure The enclosure for the device is a Hammond 1591 XXM plastic enclosure. It has an area similar to that of a deck of cards, and a height of two decks. The spectrometer is the tallest component with the height of 10.1 mm. The volume of the enclosure could be halved using a stack of two smaller boards, with a combined height of around 10 mm. The additional benefit from that is the possibility to dedicate one board for analog signals and another for digital signals. However,

in this prototype this wasn't necessary since even with a single PCB the device is small enough to fit in a hand.

Design errors Since the second prototype was working correctly, the design process of the third prototype was mostly just copying the breadboard circuit and the relevant parts of the microcontroller evaluation board to a custom PCB. Nevertheless, the PCB had a few design errors: three missing traces and a mirrored programming connector pinout, all of which were careless mistakes. The layout shown in Figure 11 contains these errors. The missing traces were fixed using short jumper wires, and the programming cable was rewired to match the erroneous pinout.

One error that was present in the second prototype was copied over to the third prototype. The buffer amplifier does not have a rail-to-rail input, yet its supply voltage was the same as the highest input voltage, 5 V. As a result, the amplifier limited the signal level to around 4 V. This was not noticed while using the second prototype, as it had a trimmer potentiometer as a voltage divider. On the second prototype the signal was limited to 4 V as well, but the trimmer was adjusted so that the signal that went to the ADC was 3.3 V. This resulted in a loss of dynamic range. The third prototype replaces the trimmer with fixed resistors, which were calculated to divide 5 V to 3.3 V, and the error was found.

There were two possible solutions for this problem, either using a higher supply voltage for the buffer amplifier or replacing the amplifier altogether. No suitable replacement for the amplifier was found, as it should have matching performance and both rail-to-rail input and output. Instead, it was decided to use a higher supply voltage, as 10 V from the charge pump was readily available. This was lowered to 7 V using an LM1117 linear regulator. Since there was no space on the PCB, components were soldered on a small protoboard which was wired to the PCB.

5.4.2 Software on the microcontroller

The software developed for the second prototype was mostly complete. An addition to the software was an ability to configure the measurement parameters, such as exposure time, over the serial connection. On the previous prototypes the parameters were fixed.

As the device was used, it was noticed that the automatic exposure control is too slow. To fix this, a new control method was devised. Two values have been predefined, a target level and an overexposure level. If a single pixel is above the overexposure level, the complete measurement is considered as overexposed. In that case the exposure time is lowered to 33 % of the original value and the

measurement is repeated. Otherwise the target level is divided by the highest value in the measurement, and the original exposure time is multiplied by the result. This way the exposure time of the next measurement is closer to the optimal.

With the new control method, the delay between a change in lighting conditions and the device having a suitable exposure time was greatly reduced.

5.4.3 Software on the PC

The software on the PC (Fig. 12) was developed heavily, as the device was demonstrated to the potential customers. The software has now the following features:

Graphical user interface Whereas the previous version only displayed a plot of the spectrum, this version includes full control of measurement parameters. The interface was made using TkInter, as it is included in the default Python installation [55].

Displays either a raw or a corrected spectrum The spectrum is corrected by subtracting dark noise and applying a spectral response correction.

Ability to save the measurement data The measurement data is saved in a CSV format. CSV was chosen as it is a simple format and readable by both humans and spreadsheet programs.

Supports several spectrometer modules Hamamatsu had supplied two spectrometer modules for prototyping, and the idea was to use both of them for measurements. Since the spectrum correction is done on the PC, the software has to contain the correction data for both spectrometers, and a way to select between them.

Calculates colorimetric values The values are calculated using Colour [14], a Python color science library. The library calculates the CIE chromaticity coordinates, the correlated color temperature and the color rendering index from the measured spectrum. The spectrum has to be corrected before calculations.

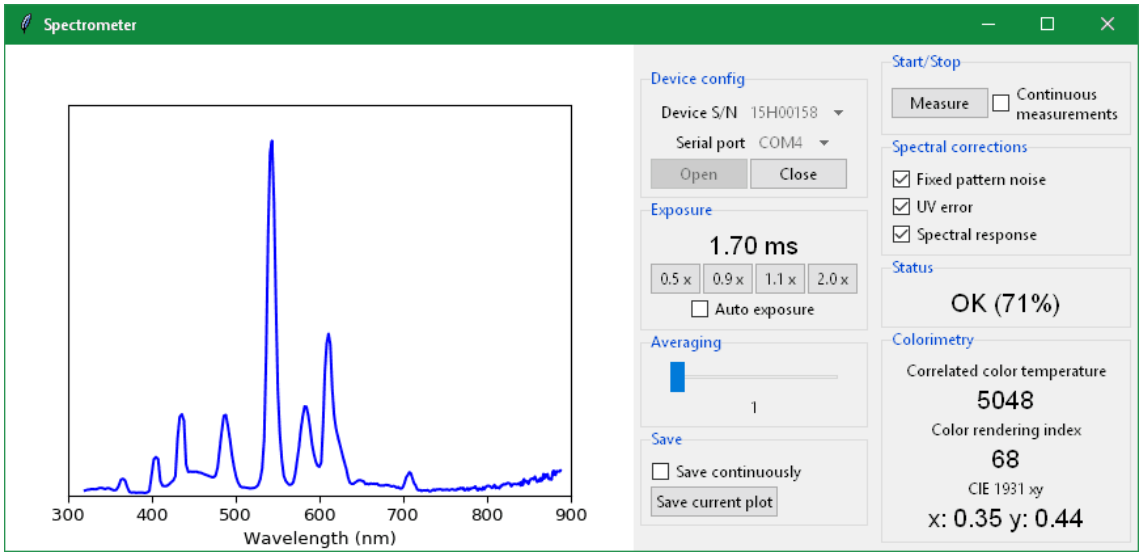

Figure 12: The final version of the PC software, displaying the spectrum of a fluorescent light.

6 Calibration and measurements

As with every real-world measurement device, the spectrometer used in this thesis, Hamamatsu C12880MA, is far from ideal. It has nonlinearities in spectral response and spectral resolution, to name a few. On top of that, also the AD conversion and the electronics related to that have their own nonlinearities. These nonlinearities have to be known as well as possible, since that information is used for calibrating the device and to correct the measurement results.

> The objective of a calibration is to make measurement results independent of the particular measuring instrument or measuring technique employed. In other words, it is desired that when the same magnitude of a physical quantity is measured by different instruments at different times and/or places, and possibly by different methods, the resulting values should always be the same. [46, p. 2]

The principle of operation for image sensors is converting incident photons to electrons. When a photon of sufficient energy is absorbed by a semiconductor material, one or multiple electrons are excited to a higher-energy state, which eventually creates a small electric current. [63, p. 106, 30, p. 11]

The first step for calibrating the spectrometer is knowing the major sources of error, which are output offset voltage, dark current signal, and spectral response of the sensor. [58]

For the measurements, two different Hamamatsu C12880MA spectrometers were used, serial numbers 15H00158 and 15H00160. In this chapter, these are referred as “58” and “60”, respectively. Every measurement, excluding Figure 13, has the dark noise subtracted from the measurement.

6.1 Offset voltage and dark current

Output offset voltage is caused by variations in the semiconductor. In CMOS sensors each pixel has a different offset level, but the offset level of a certain pixel varies from one sensor array to another. The offset level varies also as a function of temperature. [30, p. 186, 58] Hamamatsu specifies that the level of the offset voltage on a C12880MA spectrometer varies between 0.3 V and 0.9 V [26]. The bulk of the offset can be removed using a subtracting op-amp circuit, as Hamamatsu has done in the C13016 evaluation board [27]. The offset can be also removed digitally after the AD conversion, but the benefit of using an op-amp for subtracting is the better use of the dynamic range of the ADC. In the device described in this thesis the offset is removed digitally, due to the simplicity of the method.

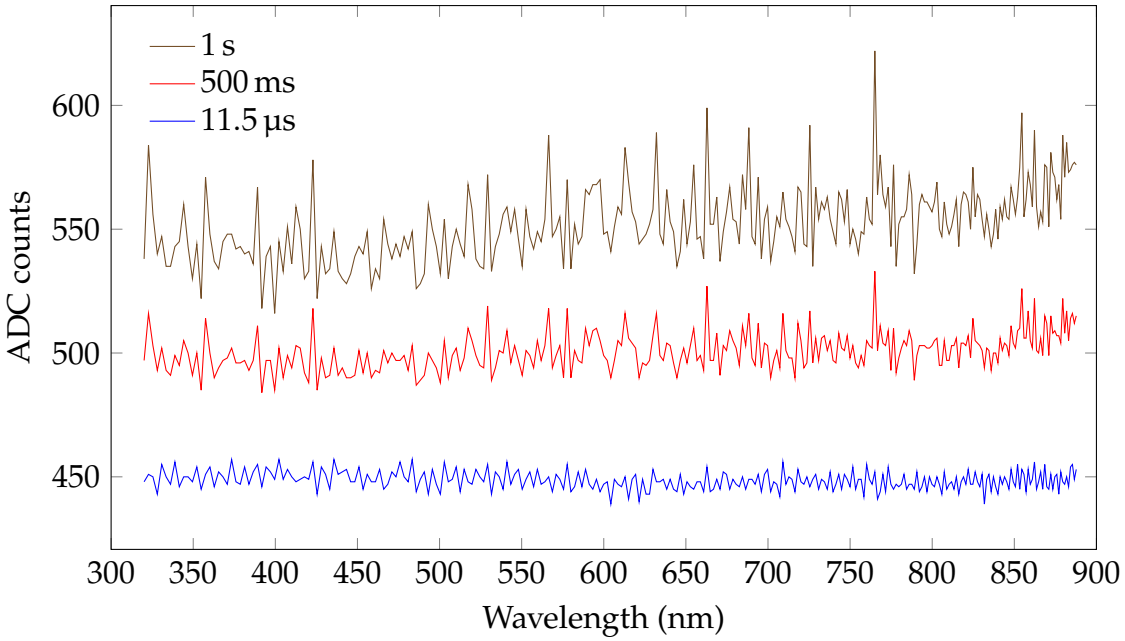

Figure 13: Output offset voltage and the effect of exposure time on dark noise. At the shortest exposure time, 11.5 µs, the output offset voltage is the main source of the signal. Since each pixel has a slightly different offset, the measured signal has a notable error pattern. As the exposure time increases, the signal caused by dark current becomes more prominent. On average the dark current noise increases linearly with the exposure time, but there are also a few non-linear pixels. Similar non-linear behavior was noted also by Schöberl et al. [58]. Note that the range of ADC counts is 0–4095. The measurements were made using the "58" spectrometer.

Dark current is a small leakage current that produces a charge in the pixels of the sensor even when there are no incident photons. The amount of dark current depends on the exposure time and the sensor temperature. There are several sources for dark current, but thermally generated dark current is the most common one. [30, pp. 167, 170, 58].

Each pixel of the sensor has a different amount of offset voltage and dark current, as shown in Figure 13, but those also vary from device to device [30, p. 186, 58]. This dark noise has to be removed from the signal before correcting the spectral response, otherwise the noise signal will be amplified by the spectral response correction [73, p. 92]. The most effective way would be measuring the dark noise right before the actual measurement, but since the device has no shutter, the amount of dark noise has to be modeled. As stated previously, the amount of dark current depends on the exposure time and the sensor temperature. The range of the sensor temperature in a typical usage is minor compared to the range of the exposure time, thus temperature sensing was deemed unnecessary at the prototype stage.

The dark noise of each pixel was modeled using a simple linear fitting, mentioned in [58]:

$$N_{dark} = i_{dark} \cdot t_{exp} + V_{offset} \tag{11}$$

where i_{dark} is dark current, t_{exp} exposure time and V_{offset} offset voltage.

The dark noise of each spectrometer was measured by first covering the window of the spectrometer with a piece of copper tape and then measuring the signal. The exposure times ranged from 11.5 µs to 1 s, and the final measurement of each exposure was an average of 50 measurements, in order to minimize the amount of dynamic noise in the measurements.

Measured data was processed with SciPy's [31] linear regression function, which gave the values for i_{dark} and V_{offset} for each pixel. This model was used to correct the measurements: the modeled dark noise was subtracted from the measurement in order to get a measurement with no dark noise.

As Figure 13 shows, some pixels behave non-linearly. Schöberl et al. [58] suggest that a segmented linear model is more accurate for modeling non-linear behavior, but the linear model was deemed sufficient for prototyping, since the amount of non-linearity is quite small.

6.2 Spectral response

The image sensor's ability to convert photons of different energies to electrons is called quantum efficiency. Quantum efficiency depends on the energy of the photon, and thus on the wavelength. Consequently, the wavelength of the photon determines how large charge is generated. This is expressed as spectral response (Fig. 14). [63, p. 108]

In order to get measurements that correspond to a real-world situation, the spectral response has to be known beforehand. This can be determined by measuring the spectrum of a calibration lamp. The spectral response can be calculated when both the measured spectrum and the actual spectrum are known. [21]

The first measurement was made using Ocean Optics HL-2000-CAL tungsten-halogen calibration light source (Fig. 15). The measurement had two unexpected sources of error, out-of-band response and internal stray light, both of which are visible in Figure 15.

As the tungsten filament has approximately the same spectrum as a blackbody radiator [74, p. 15], and the spectrum of the light source was known from 350 nm to 1100 nm, it was clear that the measured UV levels were unrealistically high, especially considering how low the response of the sensor was at UV range. As the

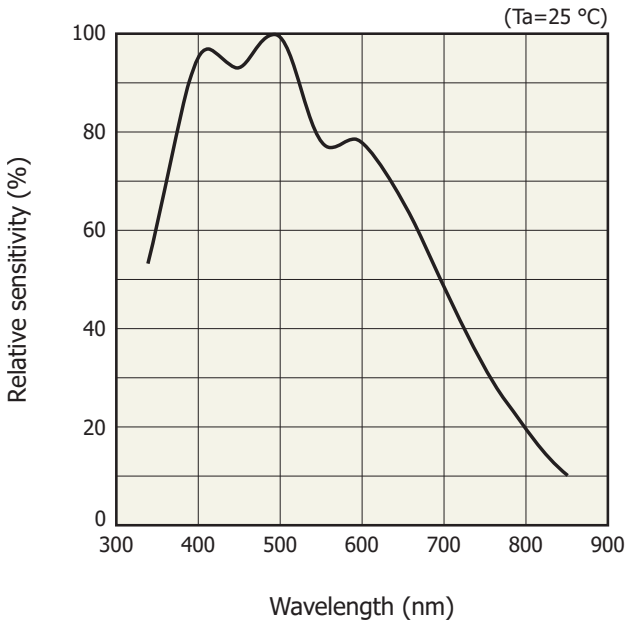

Figure 14: The typical spectral response of Hamamatsu C12880MA spectrometer. (Image reproduced with permission of Hamamatsu Photonics) [26]

light sources used in testing thus far had been LEDs and fluorescent lights, this behavior had not been noticed before.

A likely reason for the out-of-band response was overlapping of diffracted spectrums. Diffraction gratings form not only one, but several diffraction patterns called orders. Each order is diffracted in a different direction, but if the patterns are wide enough, there can be overlap. [54, pp. 20–28] Within the spectrometer, one of these orders is measured with the image sensor. In this case the spectrum of the halogen lamp had radiation in such high wavelength range, that the pattern of an unwanted order overlapped the pattern of the wanted order.

This kind of out-of-band response is a problem for calibration, but it can be mitigated using an optical bandpass or shortpass filter. If a filter is used during the calibration, the same filter has to be used with the device thereafter.

Reflections and scattering within the spectrometer cause stray light that adds up to the real spectral input of the image sensor [54, p. 155]. This is visible as a reduced signal-to-noise ratio. In Figure 15 the lowest measured signal at 375 nm should be near zero, as the spectral response at that point is only about 80 % of the maximum. Reducing the amount of stray light is difficult, since almost all of the techniques suggested by Palmer and Loewen [54, pp. 167–169] require an access to the optical path of the spectrometer module, which is in this case a sealed component. The only executable suggestion is to use a filter in front of the spectrometer to eliminate out-of-band wavelengths.

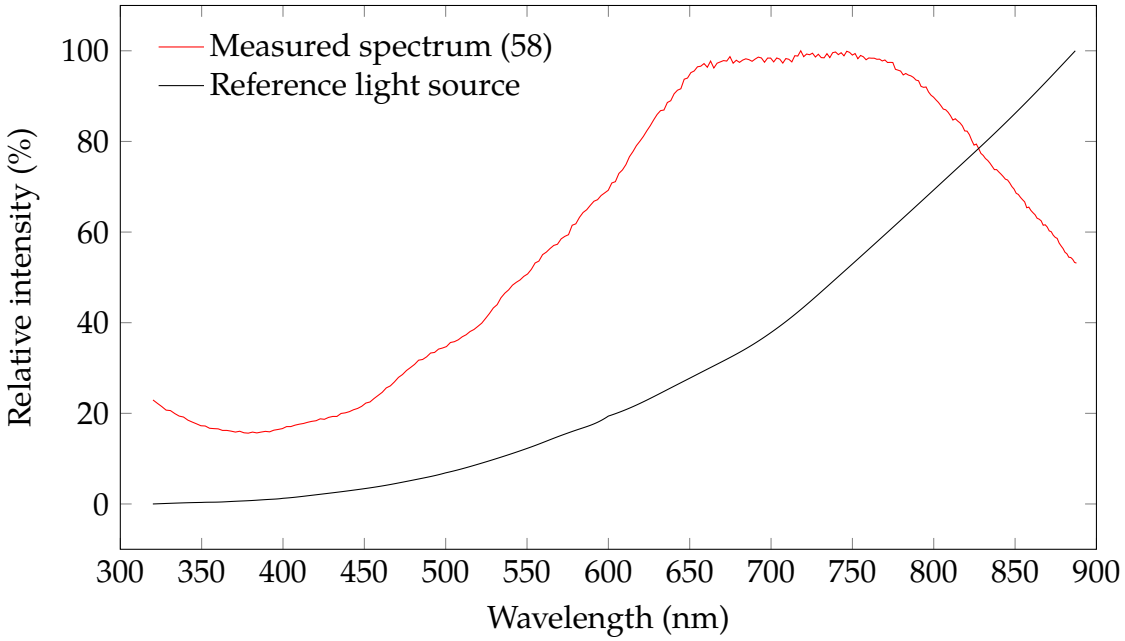

Figure 15: The spectrum of Ocean Optics HL-2000-CAL tungsten-halogen calibration light source. Note how at 320 nm to 375 nm the measured spectrum rises as the wavelength shortens, even though both the real spectrum and the spectral response (Fig. 14) are declining. This can be explained by the limitations of the optical setup in the spectrometer module.

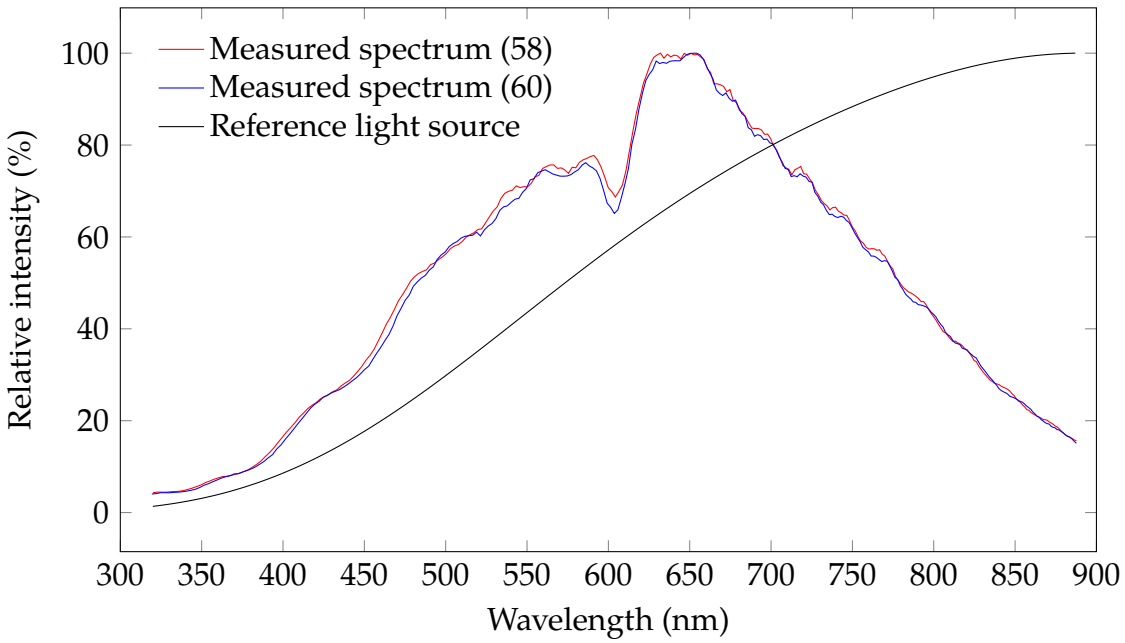

Figure 16: The spectrum of an irradiance standard FEL lamp. When compared to Figure 15, there is no out-of-band response visible at wavelengths under 375 nm, and the lowest measured value is closer to zero.

The influence of stray light was also tested using a laser pointer. If the laser beam was positioned correctly, a stray light error was visible throughout the measured spectrum. The level of the error depended on the input angle of the laser beam. This underlines the shortcomings of this compact and relatively low-cost Hamamatsu C12880MA spectrometer module.

The second measurement was made using an irradiance standard FEL lamp (Fig. 16). The FEL lamp was positioned 50.0 cm from the spectrometer. Baffles were placed between the lamp and the spectrometer and also around the spectrometer, to lower external stray light reaching the spectrometer. This time the measurements had no signs of out-of-band error and fewer signs of internal stray light. This was likely due to the higher color temperature of the FEL lamp compared to Ocean Optics HL-2000-CAL. As the color temperature rises, the amount of infrared radiation compared to visible radiation reduces.

6.3 Linearity

The linearity of a spectrometer measures how consistently a change in the measurement matches a change in the measured light. Hamamatsu specifies that the typical error in linearity is between 0 % and −8 % from the ideal value, when exposure times range from 1 ms to 700 ms [26].

The linearity was measured using two different methods, by varying the exposure time while keeping the intensity of the light constant, and vice versa. In both cases, each data point was an average of the measured spectrum. This way the relative change between the measurements could be calculated, without knowing any specifics of the spectrum. The test setup was the same as on the second spectral response measurement using the FEL lamp, but with the spectrometer mounted on a linear slide.

Linearity relative to light intensity (Fig. 17) was measured by keeping the light source and the exposure time constant and varying the distance between the lamp and the spectrometer. As the intensity follows the inverse-square law, the relative change in light intensity between distances could be calculated. The maximum deviation from the ideal was (-2.5 ± 0.5) %. The known contribution to the uncertainty came from the distance adjustment. The measurement was made using only the “58” spectrometer since the “60” had some temperature problems when using the FEL lamp. These problems are detailed in Section 6.5.

Linearity relative to exposure time (Fig. 18) was measured by keeping the light source and the distance constant and varying the exposure time. The maximum deviation from the ideal was −2.1 % for the “58” and −0.9 % for the “60”. The amount of uncertainty could not be estimated for this measurement, but it is assumed to be minimal. More interestingly, this measurement revealed that the

slope of the linearity was different between the spectrometers, which is something that has to be considered when calibrating the spectral response.

6.4 Spectral accuracy and resolution

Each pixel on the sensor of the spectrometer corresponds to a certain wavelength. Hamamatsu has measured this for each C12880MA spectrometer and supplies the information with the spectrometer as a fifth-degree polynomial. This polynomial is wavelength as a function of pixel number.

A monochromatic light shows as a peak, but the light will fall on several pixels, and thus it will show as a wider peak than it is in reality. If two peaks are too close to each other, they cannot be distinguished from each other. The spectrometer's spectral resolution, or the ability to resolve two wavelengths, depends typically on the diffraction grating, but also on a few other factors [54, p. 33]. The higher the resolution, the narrower is the peak that the monochromatic light forms.

The accuracy of the wavelength polynomial and the spectral resolution of the spectrometer was measured using Ocean Optics HG-1 mercury argon calibration lamp. It is a wavelength source which spectrum consists of several narrow peaks. Figure 19 shows the wavelengths of those peaks as vertical lines.

The measurement data, plotted in Figure 19, shows that the full width at half maximum (FWHM) of those peaks is about 10 nm. Hamamatsu has specified the typical spectral resolution as 12 nm [26].

There is no specification for the wavelength accuracy, but the data shows small variations between the two spectrometers. For example the 365.0 nm peak from the reference source shows at 364.0 nm on both spectrometers, but the 435.8 nm peak shows at 434.0 nm on the "58" and at 436.5 nm on the "60". These results were obtained by interpolating the spectral data using Sprague interpolation [72]. The resolution of the interpolated data was 0.5 nm.

6.5 Additional notes

The spectrum of the sun was measured by pointing the spectrometer towards the sun. Measurements were made using the shortest exposure time possible, 54 cycles which equals, in this case, 11.5 µs. As the sampling rate was 4.7 MSPS and the calculated requirement was 3.3 MSPS (see Section 5.1), the spectrometer was expected to pass the test with flying colors. In reality the measurement was severely clipped. Later analysis showed that the exposure time should have been approximately 5 times shorter in order not to overexposure the measurement. The reason for this is not completely understood, but it is probably related to

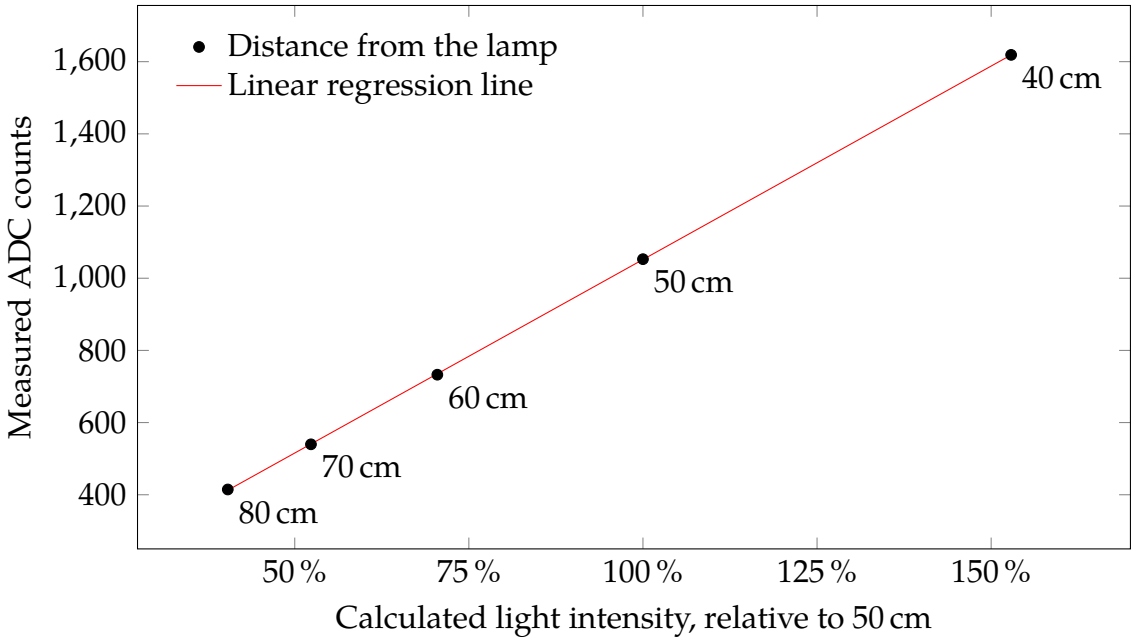

Figure 17: Spectrometer linearity relative to light intensity. The intensity of the light was changed by varying the distance between the FEL lamp and the spectrometer, while keeping the exposure time constant. As the intensity follows the inverse-square law, the relative change between distances can be calculated. Measurements were made using the "58" spectrometer.

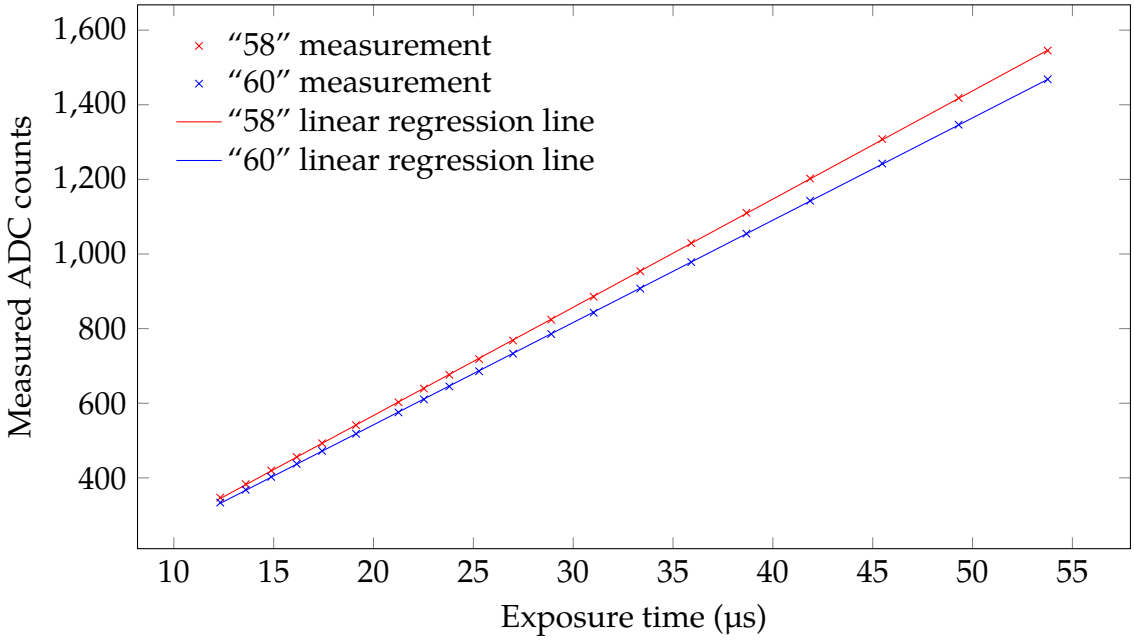

Figure 18: Spectrometer linearity relative to exposure time. The exposure time was varied while the intensity of the light was kept constant. Even though both of the spectrometers are linear relative to exposure time, the slope differs.

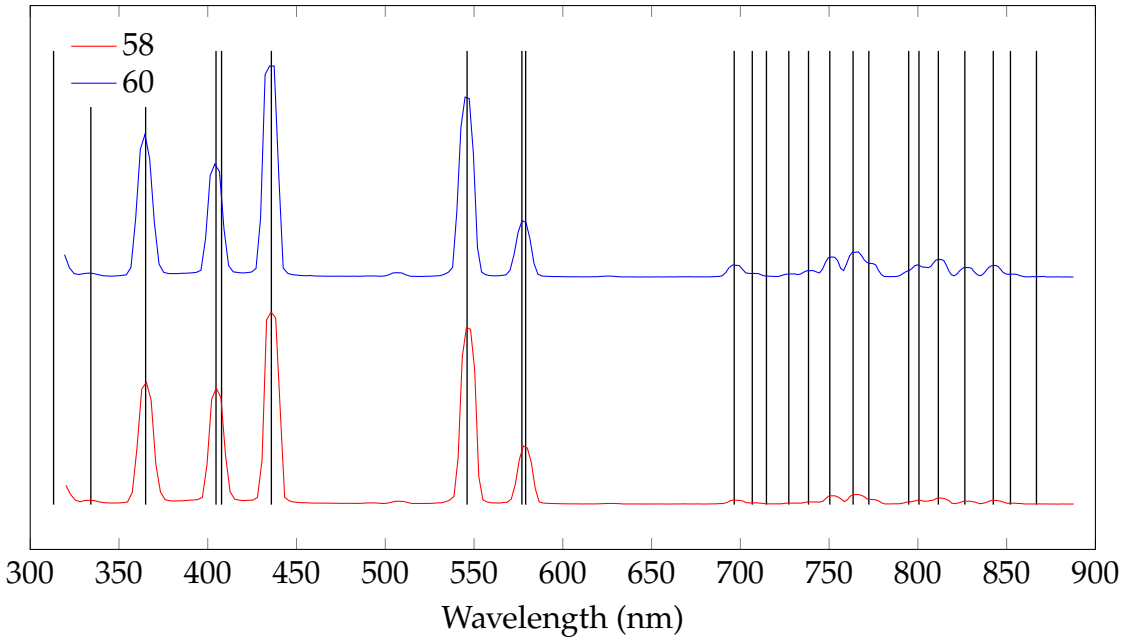

Figure 19: The emission spectrum of Ocean Optics HG-1 mercury argon calibration lamp, measured with both "58" and "60" spectrometers. The vertical lines represent the wavelengths present in the spectrum and their known locations.

how Hamamatsu determines the maximum incident light level [26, p. 4]. As the illuminance level of sun is about 80 000 lx, the highest illuminance level the spectrometer can measure is approximately 17 000 lx [12, p. 19]. The exposure time of the spectrometer can be as high as 700 ms before the linearity suffers, which means the lowest light it can measure should be 0.3 lx. The measurement range is comparable to the commercial handheld spectrometers shown in Table 1 (page 5), but the measurement range starts and ends at a lower light level than the devices in the table.

The temperature problems encountered with the "60" spectrometer were due to external heating by the 1000 W FEL lamp. If the operating temperature of the spectrometer rose too high, measurements were erroneous. At the time the errors were not linked to the temperature. Later on, the spectrometer module was heated with a small incandescent bulb, and when the surface temperature of the spectrometer module was around 45–50 °C or higher, similar errors were observed. Hamamatsu specifies the operating temperature range as 5 °C to 50 °C. Both "58" and "60" spectrometers had similar symptoms in high temperatures, the difference was that the "58" required a higher temperature than the "60" before the errors appeared.

7 Conclusions

The aim of this study was to prototype electronics and software for a Hamamatsu C12880MA spectrometer module. The spectrometer module itself is a small, hermetically sealed unit that contains the necessary optical parts and an image sensor chip.

The requirements for the device were:

- measures the spectrum of visible light on a broad range of light intensities
- is small and lightweight
- the electronics are customizable according to customers' needs
- has a minimal user interface on the device itself
- has an extensive user interface on a PC or a mobile device.

The requirements were met by designing a device and software that interfaces with the spectrometer, digitizes the measured spectrum, and transfers it to a computer. This was done using an ARM-based microcontroller, which contained several necessary peripherals for interfacing with the spectrometer module. Software on the computer displays the spectrum and colorimetric values related to it. As the electronics and the software are self-developed, later customizations are possible. The capabilities of the device were tested by measuring various reference light sources, and the results showed that, for the most part, the device was working as expected.

7.1 Alternative routes

The most difficult and time-consuming part was getting the spectrometer module and the supporting components to operate at high speed. The high speed made it possible to have a wide dynamic range, as the shortest exposure time could be made shorter. The chosen solution was to use a fast microcontroller with a fast on-chip ADC. Using an integrated ADC simplified developing, but the accuracy of the ADC was a limiting factor.

The manufacturer of the spectrometer module has an evaluation board for the spectrometer, where they have used a proper high-performance ADC and an FPGA. This is to ensure that the factor that holds back the performance is the spectrometer itself, not the supporting electronics. As developing the software for the microcontroller was difficult enough, using an FPGA would have been out of the question.

A more feasible route would have been to keep using the parts selected for the first prototype, despite the longer exposure times. The stand-alone ADC would have had a higher accuracy and the development might have been easier since now the high speed brought with it several edge cases. If a possibility for measuring bright lights had been needed, a neutral-density filter could have been used. Using a filter limits the low-light usage since linearity of the spectrometer drops when long exposure times are used. This is why the high speed was required for maximizing the dynamic range.

7.2 Further development

As the spectrometer developed in this study is meant to be customizable according to the needs of the customer, there isn't a certain plan for future development.

Most of the possible additions are related to the measurement process. Including a temperature sensor and a mechanical shutter would reduce the error caused by dark noise. Currently, the dark noise pattern is not measured right before the actual measurement, and the effect of temperature is not taken into account when subtracting the dark noise. An optical shortpass filter would help with out-of-band response problems, which may occur when measuring light sources with high infrared content, such as incandescent bulbs. Neutral-density filter would allow measuring brighter light sources, such as the sun. If requested a radiometric calibration could be made with traceability to a primary standard.

If a hand-held operation is required, the device could be fitted with a wireless communication module and a rechargeable battery. Another addition could be a cosine corrector, which is an optical diffuser that widens the field of view of the spectrometer.

Additional measurements, made using several devices, would give more information about the accuracy and the limitations of the device. These measurements could include EMC testing, to find out how much the electronics emit electromagnetic radiation and how sensitive they are to it.

References

[1] Allied Scientific Pro. *Lighting Passport*. 2017. URL: http://www.lightingpassport.com/ (visited on 2017-05-11).

[2] Analog Devices. *AD7944 datasheet, "14-Bit, 2.5 MSPS, PulSAR, 15.5 mW ADC in LFCSP"*. 2016-02. URL: http://www.analog.com/media/en/technical-documentation/data-sheets/AD7944.pdf (visited on 2016-10-27).

[3] ARM. *Cortex-M0+ Technical Reference Manual*. 2012. URL: http://infocenter.arm.com/help/topic/com.arm.doc.ddi0484c/DDI0484C_cortex_m0p_r0p1_trm.pdf.

[4] Atmel. *Appl. Note AVR120: Characterization and Calibration of the ADC on an AVR*. 2016-08-17.

[5] Atmel. *Appl. Note AVR121: Enhancing ADC Resolution by Oversampling*. 2005-09-01.

[6] Atmel. *ATmega48A/PA/88A/PA/168A/PA/328/P Datasheet, "Atmel 8-Bit Microcontroller with 4/8/16/32K Bytes of In-System Self-Programmable Flash Progam Memory"*. 2014-10. URL: http://www.atmel.com/images/Atmel-8271-8-bit-AVR-Microcontroller-ATmega48A-48PA-88A-88PA-168A-168PA-328-328P_datasheet_Complete.pdf (visited on 2015-11-30).

[7] Atmel. *AVR 8-Bit Instruction Set*. 2014-07. URL: http://www.atmel.com/images/atmel-0856-avr-instruction-set-manual.pdf (visited on 2015-12-16).

[8] Atmel. *SAM D09 Preliminary Datasheet, "SMART ARM-Based Microcontroller"*. 2015-08. URL: http://www.atmel.com/Images/Atmel-42414-SAM-D09_Datasheet.pdf (visited on 2015-11-30).

[9] B&H Photo Video. *Gossen MAVOSPEC BASE Industrial Light Meter*. 2017. URL: https://www.bhphotovideo.com/c/product/1317251-REG/gossen_go_m521g_mavospec_base_light_meter.html (visited on 2017-05-11).

[10] B&H Photo Video. *Ikan CV600 Chrome View Spectrometer*. 2017. URL: https://www.bhphotovideo.com/c/product/1244777-REG/ikan_cv600_chrome_view_spectrometer.html (visited on 2017-05-11).

[11] D. Thorburn Burns. "Aspects of the Development of Colorimetric Analysis and Quantitative Molecular Spectroscopy in the Ultraviolet-Visible Region". In: *Advances in Standards and Methodology in Spectrophotometry*. Ed. by C. Burgess and K. D. Mielenz. Vol. 2. Analytical Spectroscopy Library. Elsevier, 1987, pp. 1–19. ISBN: 978-0-444-42880-6.

[12] Theodore W. Cannon. "Light and Radiation". In: *Handbook of Applied Photometry*. Ed. by Casimer DeCusatis. Woodbury, N.Y. : Washington, DC: AIP Press, 1997, pp. 1–31. ISBN: 978-1-56396-416-9.

[13] Ivan Chew et al. "A Spectrally Tunable Smart Led Lighting System with Closed-Loop Control". In: *IEEE Sensors Journal* 16.11 (2016), pp. 4452–4459. URL: http://ieeexplore.ieee.org/abstract/document/7433935/.

[14] *Colour: Colour Science for Python*. 2017-06-01. URL: https://github.com/colour-science/colour (visited on 2017-06-01).

[15] Anshuman J. Das et al. "Ultra-Portable, Wireless Smartphone Spectrometer for Rapid, Non-Destructive Testing of Fruit Ripeness". In: *Scientific Reports* 6 (2016-09-08). DOI: 10.1038/srep32504.

[16] Joe Desbonnet. *LPC824_ADC_DMA_example: A Example Program to Read NXP LPC824 ADC into SRAM Using DMA*. 2017-01-19. URL: https://github.com/jdesbonnet/LPC824_ADC_DMA_example (visited on 2017-05-22).

[17] Edmund. *Laboratory Spectrometer*. 2017. URL: https://www.edmundoptics.com/testing-detection/spectroscopy/Laboratory-Spectrometer-88406/#specs (visited on 2017-05-12).

[18] Mario Edno. *Voltage Reference Selection Basics*. 2014.

[19] P. Fara. "Newton Shows the Light: A Commentary on Newton (1672) 'A Letter ... Containing His New Theory about Light and Colours...'" In: *Philosophical Transactions of the Royal Society A: Mathematical, Physical and Engineering Sciences* 373.2039 (2015-03-06). DOI: 10.1098/rsta.2014.0213.

[20] Ingar Fredriksen and Pal Kastnes. *Choosing a MCU for Your next Design; 8 Bit or 32 Bit?* Atmel, 2014. URL: http://www.atmel.com/images/45107a-choosing-a-mcu-fredriksen_article_103114.pdf (visited on 2015-12-07).

[21] A. K. Gaigalas et al. "Procedures for Wavelength Calibration and Spectral Response Correction of CCD Array Spectrometers". In: *Journal of Research of the National Institute of Standards and Technology* 114.4 (2009), pp. 215–228. DOI: 10.6028/jres.114.015.

[22] Gigahertz-Optik. *MSC15 Low Cost Spectral Light Meter*. 2017. URL: http://www.gigahertz-optik.de/en-us/product/msc15#_specification (visited on 2017-05-11).

[23] GOSSEN. *GOSSEN MAVOSPEC BASE*. 2017. URL: http://gossen-photo.de/english/spektro_p_mavospec-base.php (visited on 2017-05-11).

[24] S. Haenzsche, S. Henker, and R. Schüffny. "Modelling of Capacitor Mismatch and Non-Linearity Effects Ini Charge Redistribution SAR ADCs". In: *Proceedings of the 17th International Conference Mixed Design of Integrated Circuits and Systems - MIXDES 2010*. 2010-06, pp. 300–305.

[25] Liisa Halonen and Jorma Lehtovaara. *Valaistustekniikka*. Otatieto 542. Espoo: Otatieto, 1992. ISBN: 978-951-672-145-6.

[26] Hamamatsu. *C12880MA Datasheet, "Finger-Tip Sized, Ultra-Compact Spectrometer Head Supporting High Sensitivity and Long Wavelength Region"*. 2015-10. URL: http://www.hamamatsu.com/resources/pdf/ssd/c12880ma_kacc1226e.pdf (visited on 2015-11-24).

[27] Hamamatsu. *C13016 Reference Document*. 2015.

[28] Paul Horowitz and Winfield Hill. *The Art of Electronics*. 3rd. New York, NY: Cambridge University Press, 2015-04-09. 1220 pp. ISBN: 978-0-521-80926-9.

[29] John D. Hunter. "Matplotlib: A 2D Graphics Environment". In: *Computing in Science & Engineering* 9.3 (2007), pp. 90–95. DOI: 10.1109/MCSE.2007.55.

[30] James R. Janesick. *Photon Transfer*. Bellingham, Washington: SPIE, 2007. 276 pp. ISBN: 978-0-8194-6722-5.

[31] Eric Jones, Travis Oliphant, Pearu Peterson, et al. *SciPy: Open Source Scientific Tools for Python*. 2001. URL: http://www.scipy.org/.

[32] Walt Jung and Walt Kester. "Hardware Design Techniques - Analog Power Supply Systems". In: *Data Conversion Handbook*. Ed. by Walt Kester. Analog Devices series. Amsterdam ; Boston: Newnes, 2005. ISBN: 978-0-7506-7841-4.

[33] Walt Kester. "ADC Input Noise: The Good, The Bad, and The Ugly. Is No Noise Good Noise?" In: *Analog Dialogue* 40.1 (2006-02), pp. 13–17. URL: http://www.analog.com/en/analog-dialogue/articles/adc-input-noise.html.

[34] Walt Kester and James Bryant. "ADC Architectures". In: *Analog-Digital Conversion*. Ed. by Walt Kester. Analog Devices, 2004. ISBN: 978-0-916550-27-1.

[35] Walt Kester, Dan Sheingold, and James Bryant. "Fundamentals of Sampled Data Systems". In: *Data Conversion Handbook*. Ed. by Walt Kester. Analog Devices series. Amsterdam ; Boston: Newnes, 2005. ISBN: 978-0-7506-7841-4.

[36] Robert Kollman and John Betten. "Powering Electronics from the USB Port". In: *Texas Instruments Analog Applications Journal* (2002 2Q). URL: http://www.ti.com/lit/an/slyt118/slyt118.pdf.

[37] Konica Minolta Sensing. *CL-70F CRI Illuminance Meter*. 2017. URL: http://sensing.konicaminolta.us/products/cl-70f-illuminance-meter/ (visited on 2017-05-11).

[38] Takao Kuroda. *Essential Principles of Image Sensors*. CRC Press, 2014-08-12. 196 pp. ISBN: 978-1-4822-2005-6.

[39] James A Langbridge. *Professional Embedded ARM Development*. Hoboken, N.J.: Wiley, 2014. ISBN: 978-1-118-88782-0.

[40] Daniel Malacara. *Color Vision and Colorimetry: Theory and Applications, Second Edition*. Bellingham, Washington: SPIE, 2011-07-12. ISBN: 978-0-8194-8397-3.

[41] Maxim Integrated. *The ABCs of ADCs: Understanding How ADC Errors Affect System Performance*. 2002-07-22. URL: https://www.maximintegrated.com/en/app-notes/index.mvp/id/748.

[42] William Ross McCluney. *Introduction to Radiometry and Photometry*. Boston: Artech House, 1994. 402 pp. ISBN: 978-0-89006-678-2.

[43] Microchip. *PIC18F2XK20/4XK20 Datasheet, "28/40/44-Pin Flash Microcontrollers with XLP Technology"*. 2015. URL: http://ww1.microchip.com/downloads/en/DeviceDoc/40001303H.pdf (visited on 2015-12-07).

[44] Shridhar Atmaram More. *ADC Performance Parameters - Convert the Units Correctly!* Texas Instruments, 2013-05.

[45] Isaac Newton. "A Letter of Mr. Isaac Newton, Professor of the Mathematicks in the University of Cambridge; Containing His New Theory about Light and Colors: Sent by the Author to the Publisher from Cambridge, Febr. 6. 1671/72; In Order to Be Communicated to the R. Society". In: *Philosophical Transactions of the Royal Society of London* 6 (69-80 1671-01-01), pp. 3075–3087. DOI: 10.1098/rstl.1671.0072.

[46] Fred E. Nicodemus and George J. Zissis. *Methods of Radiometric Calibration*. 4613-20-R. Ann Arbor, Michigan: Institute of Science and Technology (University of Michigan), 1962-10, p. 76.

[47] NXP. *LPC111x/LPC11Cxx User Manual*. 2014-06-10. URL: http://www.nxp.com/documents/user_manual/UM10398.pdf (visited on 2015-11-30).

[48] NXP. *LPC5410x Product Data Sheet*. 2016-10-03. URL: http://www.nxp.com/documents/data_sheet/LPC5410X.pdf (visited on 2016-12-14).

[49] NXP. *LPC81x User Manual*. 2014-04-02. URL: http://www.nxp.com/documents/user_manual/UM10601.pdf (visited on 2015-11-30).

[50] NXP. *LPC82x User Manual*. 2016-05-24. URL: http://www.nxp.com/documents/user_manual/UM10601.pdf (visited on 2015-11-30).

[51] Ocean Optics. *STS-VIS*. 2017. URL: https://oceanoptics.com/product/sts-vis-microspectrometer/ (visited on 2017-05-12).

[52] Claudio Oleari. *Standard Colorimetry: Definitions, Algorithms, and Software*. Chichester, West Sussex: Wiley, 2016. 493 pp. ISBN: 978-1-118-89444-6.

[53] Henry W. Ott. *Electromagnetic Compatibility Engineering*. Hoboken, N.J: Wiley, 2009-09. 872 pp. ISBN: 978-0-470-18930-6.

[54] Christopher Palmer and Erwin Loewen. *Diffraction Grating Handbook*. 6th. Newport Corporation, 2005.

[55] Python Software Foundation. *25.1. Tkinter — Python Interface to Tcl/Tk*. 2017. URL: https://docs.python.org/3/library/tkinter.html (visited on 2017-07-20).

[56] Marta Ramírez-Pérez et al. "Cost-Effective Hyperspectral Transmissometers for Oceanographic Applications: Performance Analysis". In: *Sensors* 15.9 (2015-08-26), pp. 20967–20989. DOI: 10.3390/s150920967.

[57] János Schanda. "CIE Colorimetry". In: *Colorimetry: Understanding the CIE System*. Ed. by János Schanda. Wiley, 2007. ISBN: 978-0-470-04904-4.

[58] M. Schöberl et al. "Non-Linear Dark Current Fixed Pattern Noise Compensation for Variable Frame Rate Moving Picture Cameras". In: *2009 17th European Signal Processing Conference*. 2009-08, pp. 268–272.

[59] E. Fred Schubert. *Light-Emitting Diodes*. Cambridge; New York: Cambridge University Press, 2006. 422 pp. ISBN: 978-0-511-34476-3.

[60] Spectrecology. *STS-VIS Sub Miniature Fiber Optic Spectrometer*. 2017. URL: http://www.shop.spectrecology.com/STS-VIS-Sub-miniature-fiber-optic-spectrometer-STS-VIS.htm (visited on 2017-05-12).

[61] STMicroelectronics. *AN1636 - Understanding and Minimising ADC Conversion Errors*. 2003.

[62] V. V Sushkov. "Differential Non-Linearity Compensation in ADCs Employing Charge Redistribution in an Array of Binary Weighted Capacitors". In: *Nuclear Instruments and Methods in Physics Research Section A: Accelerators, Spectrometers, Detectors and Associated Equipment* 450.1 (2000-08-01), pp. 119–126. DOI: 10.1016/S0168-9002(00)00245-X.

[63] Motohiro Suyama. "Optoelectronic Sensors". In: *Handbook of Optical Metrology: Principles and Applications*. Ed. by Toru Yoshizawa. 1st. Boca Raton: CRC Press, 2009, pp. 105–135. ISBN: 978-0-8493-3760-4.

[64] Texas Instruments. *Understanding Data Converters*. 1995.

[65] Thorlabs. *CCS Series Operation Manual*. 21-Mar-2014.

[66] Thorlabs. *CCS100 - Compact Spectrometer, 350 - 700 Nm*. 2017. URL: https://www.thorlabs.com/thorproduct.cfm?partnumber=CCS100#ad-image-0 (visited on 2017-05-12).

[67] Torso-Verlag. *Spectrometer CL-70F*. 2017. URL: http://www.unitycolor.com/Testing-Technology/Light-Measurement/Spectrometer-CL-70F::517.html (visited on 2017-05-11).

[68] Gerard J. Tortora and Bryan H. Derrickson. *Principles of Anatomy and Physiology*. 14th ed. Hoboken, N.J: Wiley, 2014. 1232 pp. ISBN: 978-1-118-80843-6.

[69] UPRtek. *CV600 Spectral Color Meter*. 2017. URL: http://www.uprtek.com/s/2/product-502349/Spectral-Color-Meter-CV600.html (visited on 2017-05-11).

[70] USB Implementers Forum Inc. *Universal Serial Bus Specification Revision 2.0*. 2000-04-27.

[71] K. Uto et al. "Development of a Low-Cost Hyperspectral Whiskbroom Imager Using an Optical Fiber Bundle, a Swing Mirror, and Compact Spectrometers". In: *IEEE Journal of Selected Topics in Applied Earth Observations and Remote Sensing* 9.9 (2016-09), pp. 3909–3925. DOI: 10.1109/JSTARS.2016.2592987.

[72] Stephen Westland. "Interpolation of Spectral Data". In: *Encyclopedia of Color Science and Technology*. Ed. by Ming Ronnier Luo. Springer, 2016, pp. 794–797. DOI: 10.1007/978-3-642-27851-8_366-1.

[73] Clair L. Wyatt. *Radiometric Calibration: Theory and Methods*. New York: Academic Press, 1978. 200 pp. ISBN: 978-0-12-766150-6.

[74] Günter Wyszecki and W. S. Stiles. *Color Science: Concepts and Methods, Quantitative Data and Formulae*. 2. ed. New York: Wiley, 1982. 950 pp. ISBN: 0-471-02106-7 0-471-39918-3.

[75] Joseph Yiu. *Cortex-M for Beginners*. ARM, 2013-09.

[76] Joseph Yiu. *The Definitive Guide to ARM® Cortex®-M0 and Cortex-M0+ Processors*. 2nd. Boston, MA: Elsevier, 2015. ISBN: 978-0-12-803277-0.

[77] Joseph Yiu and Carl Williamson. *A Beginner's Guide on Interrupt Latency - and Interrupt Latency of the ARM® Cortex®-M Processors*. 2013-09-13. URL: https://community.arm.com/docs/DOC-2607 (visited on 2016-11-14).

[78] Hugh D Young, Roger A Freedman, and Lewis Ford. *University Physics with Modern Physics*. 13th. Boston, Mass.; London: Addison-Wesley, 2011. ISBN: 978-0-321-67546-0.